

UC Davis

UC Davis Previously Published Works

Title

Ketone Ester D- β -Hydroxybutyrate-(R)-1,3 Butanediol Prevents Decline in Cardiac Function in Type 2 Diabetic Mice

Permalink

<https://escholarship.org/uc/item/63984571>

Journal

Journal of the American Heart Association, 10(19)

ISSN

2047-9980

Authors

Thai, Phung N
Miller, Charles V
King, M Todd
[et al.](#)

Publication Date

2021-10-05


DOI

10.1161/jaha.120.020729

Peer reviewed

ORIGINAL RESEARCH

Ketone Ester D- β -Hydroxybutyrate-(R)-1,3 Butanediol Prevents Decline in Cardiac Function in Type 2 Diabetic Mice

Phung N. Thai , PhD; Charles V. Miller, BS; M. Todd King, MS; Saul Schaefer , MD; Richard L. Veech, MD, DPhil*; Nipavan Chiamvimonvat , MD; Donald M. Bers , PhD; Elena N. Dedkova , DVM, PhD

BACKGROUND: Heart failure is responsible for approximately 65% of deaths in patients with type 2 diabetes mellitus. However, existing therapeutics for type 2 diabetes mellitus have limited success on the prevention of diabetic cardiomyopathy. The aim of this study was to determine whether moderate elevation in D- β -hydroxybutyrate improves cardiac function in animals with type 2 diabetes mellitus.

METHODS AND RESULTS: Type 2 diabetic (db/db) and their corresponding wild-type mice were fed a control diet or a diet where carbohydrates were equicalorically replaced by D- β -hydroxybutyrate-(R)-1,3 butanediol monoester (ketone ester [KE]). After 4 weeks, echocardiography demonstrated that a KE diet improved systolic and diastolic function in db/db mice. A KE diet increased expression of mitochondrial succinyl-CoA:3-oxoacid-CoA transferase and restored decreased expression of mitochondrial β -hydroxybutyrate dehydrogenase, key enzymes in cardiac ketone metabolism. A KE diet significantly enhanced both basal and ADP-mediated oxygen consumption in cardiac mitochondria from both wild-type and db/db animals; however, it did not result in the increased mitochondrial respiratory control ratio. Additionally, db/db mice on a KE diet had increased resistance to oxidative and redox stress, with evidence of restoration of decreased expression of thioredoxin and glutathione peroxidase 4 and less permeability transition pore activity in mitochondria. Mitochondrial biogenesis, quality control, and elimination of dysfunctional mitochondria via mitophagy were significantly increased in cardiomyocytes from db/db mice on a KE diet. The increase in mitophagy was correlated with restoration of mitofusin 2 expression, which contributed to improved coupling between cytosolic E3 ubiquitin ligase translocation into mitochondria and microtubule-associated protein 1 light chain 3-mediated autophagosome formation.

CONCLUSIONS: Moderate elevation in circulating D- β -hydroxybutyrate levels via KE supplementation enhances mitochondrial biogenesis, quality control, and oxygen consumption and increases resistance to oxidative/redox stress and mPTP opening, thus resulting in improvement of cardiac function in animals with type 2 diabetes mellitus.

Key Words: cardiac function ■ roGFP2-GRX1 ■ glutathione peroxidase 4 ■ ketone bodies metabolism ■ ketone ester ■ mitochondrial permeability transition ■ mitofusin 2 ■ roGFP2-ORP1 ■ thioredoxin ■ type 2 diabetes mellitus

Type 2 diabetes (T2DM) and obesity significantly increase the risk of heart failure (HF), which is currently responsible for \approx 65% of deaths in patients with type 2 diabetes mellitus and obese patients.¹

Abnormalities in cardiac metabolism observed in T2DM can lead to a decline in contractile function and pathological left ventricular remodeling, resulting in diastolic left ventricular dysfunction known as diabetic

Correspondence to: Elena N. Dedkova, DVM, PhD, Department of Molecular Biosciences, University of California, Davis 1089 Veterinary Medicine Drive, Vet Med 3B, Suite 3009, Davis, CA 95616-8636. E-mail: ededkova@ucdavis.edu

¹In memory of Dr. Richard L. Veech, a true pioneer of keto nutrition.

Presented in part at the Biophysical Society Annual Meeting, March 2-March 6, 2019. Baltimore, Maryland.

Supplementary Material for this article is available at <https://www.ahajournals.org/doi/suppl/10.1161/JAHA.120.020729>

For Sources of Funding and Disclosures, see page 22.

© 2021 The Authors. Published on behalf of the American Heart Association, Inc., by Wiley. This is an open access article under the terms of the Creative Commons Attribution-NonCommercial License, which permits use, distribution and reproduction in any medium, provided the original work is properly cited and is not used for commercial purposes.

JAHA is available at: www.ahajournals.org/journal/jaha

CLINICAL PERSPECTIVE

What Is New?

- This study presents the first comprehensive evaluation of the effect of ketone ester D- β -hydroxybutyrate-(R)-1,3 butanediol supplementation on cardiac function in type 2 diabetes mellitus mouse model.
- This study demonstrates that a moderate elevation in circulating levels of D- β -hydroxybutyrate via ketone ester supplementation prevents progression toward diabetic cardiomyopathy in type 2 diabetic mice by limiting oxidative stress and enhancing mitochondrial quality control via mitophagy.

What Are the Clinical Implications?

- Patients with type 2 diabetes mellitus have an increased risk of developing heart failure despite the success of antihyperglycemic therapies in treating elevated serum glucose.
- Therefore, new therapies are urgently needed to prevent progression toward heart failure in patients with type 2 diabetes mellitus.
- This study demonstrates that ketone ester supplementation to induce mild ketosis in patients with type 2 diabetes mellitus could be beneficial in limiting the progression toward heart failure.

cardiomyopathy.^{2,3} Clinically, diabetic cardiomyopathy is defined as myocardial dysfunction that is not associated with coronary artery disease, valvular disease, hypertension, or cardiomyopathy of congenital/viral/familial origin.⁴ Hyperglycemia, reduced glucose oxidation, increased lipid oxidation, and insulin resistance are typical signs of the early stages of T2DM.²⁻⁵ Eventually, these changes in cardiac metabolism lead to an energetic deficit and diastolic dysfunction, before progressing to systolic dysfunction and HF with either preserved or reduced ejection fraction.^{3,6} Current treatments for T2DM have limited impact on preventing diabetic cardiomyopathy, with some even worsening this condition.^{7,8} Therefore, new therapies are needed that effectively prevent or reverse development of diabetic cardiomyopathy.

Under normal physiological conditions, cardiac myocytes use different energy substrates, including free fatty acids, carbohydrates (glucose and lactate), ketones, and amino acids, to quickly adjust substrate preference on the basis of diet, hormonal status, and altered cardiac workload.⁹ The process of oxidative phosphorylation in mitochondria generates the majority of high-energy phosphates (ATP) required to maintain contractile function. Fatty acid oxidation produces \approx 60% to 80% of total energy in the healthy heart, while the oxidation of glucose, lactate, ketone bodies, and amino acids contributes the

Nonstandard Abbreviations and Acronyms

β -OHB	β -hydroxybutyrate
$\Delta\Psi_m$	mitochondrial membrane potential
ACAT1	acetyl-CoA acetyltransferase 1
BDH1	β -hydroxybutyrate dehydrogenase
db/db	type 2 diabetic mice
FAD	flavin adenine dinucleotide
FCCP	carbonyl cyanide 4-(trifluoromethoxy)-phenylhydrazone
GPX4	glutathione peroxidase 4
GSH	reduced glutathione
GSSG	oxidized glutathione
KE	ketone ester
LC3	microtubule-associated protein 1 light chain 3
Mfn2	mitofusin 2
mPTP	mitochondrial permeability transition pore
MV	mitral valve
OCR	oxygen consumption rate
PINK1	PTEN-induced putative kinase 1
roGFP2	redox-sensitive green fluorescent protein 2
SCOT	succinyl-CoA:3-oxoacid CoA transferase
SDHB	succinate dehydrogenase
T2DM	type 2 diabetes mellitus
TCA	tricarboxylic acid

remaining 20% to 40%.^{9,10} Cardiac energy metabolism in diabetic cardiomyopathy is compromised because of impaired metabolic flexibility and mitochondrial tricarboxylic acid (TCA) cycle activity, leading to a decrease in ATP production.¹¹⁻¹⁴ Diabetic hearts cannot use glucose efficiently and rely, nearly exclusively, on the use of fatty acids as energy sources.¹⁵⁻¹⁷

Emerging evidence indicates that increased ketone body metabolism contributes to energy production in HF¹⁸⁻²¹; however, less information is available about the role of ketones in diabetic cardiomyopathy. While diabetic ketoacidosis, where ketone levels rise up to 25 mM, can be life threatening,²²⁻²⁴ a moderate elevation in circulating ketone levels could contribute to efficient energy metabolism,^{23,25} reduce oxidative stress,²⁶ and improve mitochondrial quality control via mitophagy.²⁷ In fact, a recent study showed that patients with T2DM with hyperglycemic crisis and diabetic ketosis (but not acidosis) had lower all-cause mortality when compared with those with nonketotic hyperglycemia,²⁸ suggesting that moderate ketosis could be protective in diabetes mellitus.

D- β -hydroxybutyrate (β -OHB) is the most abundant (78%) of the 3 circulating ketones, with acetoacetate

(20%) and acetone (2%) being minor.²² Ketones are generated in the liver mitochondria from nonesterified fatty acids, and then delivered to extrahepatic organs including the heart by blood circulation. The heart is the one of the major consumers of ketones, where β -OHB is oxidized in mitochondria to form acetyl-CoA. Ketogenic diets, which can elevate circulating β -OHB levels, have been used for over a century in the treatment of drug-resistant epilepsy.²⁹ However, it is difficult to maintain elevated levels of β -OHB with ketogenic diets: to achieve effective ketosis with ketogenic diets, almost complete elimination of carbohydrates is required to keep blood insulin levels low to maintain adipose tissue lipolysis. Conversely, a ketogenic diet may even induce cardiovascular complications in patients with T2DM because high-fat diets are associated with elevated lipid levels in humans and fatty liver and hepatic insulin resistance in mice.³⁰ To avoid the potential cardiovascular complications of ketogenic diets, pro-ketone D- β -hydroxybutyrate-(R)-1,3 butanediol monoester (ketone ester [KE]) was developed by Veech et al,^{31,32} which can increase plasma β -OHB levels when added to a diet. KE supplementation eliminates the need for adherence to a strict high-fat diet and does not lead to elevation in circulating free fatty acids.^{33–36} KE supplementation also makes it possible to distinguish between effects achieved by β -OHB from those related to elevation of free fatty acids. Furthermore, KE supplementation allows controlled elevation of β -OHB levels in the blood by adding differing amounts of KE to the animal diet.

The aim of the present study was to test the hypothesis that a moderate elevation in circulating β -OHB via KE supplementation improves mitochondrial and cardiac function in mice with T2DM. To test this hypothesis, mice with T2DM (db/db) and their corresponding control mice (wild-type [WT]; C57BLKS/J), were placed on a KE diet for 4 weeks. Changes in cardiac dimensions and function were monitored by in vivo echocardiography. Mitochondrial function was examined using Seahorse Extracellular Flux Analyzer and by confocal microscopy in combination with fluorescent dyes and genetically encoded fluorescent proteins. Protein expression was measured by conventional and Jess capillary western blot.

METHODS

The data that support the findings of this study are available from the corresponding author upon reasonable request. For detailed methods, please refer to Data S1.

Animals and Treatments

All animal handling and laboratory procedures were in accordance with the approved protocols of the

Institutional Animal Care and Use Committee of the University of California, Davis conforming to the *Guide for the Care and Use of Laboratory Animals* (8th Edition, 2011) published by the US National Institute of Health. Ten-week-old male db/db mice (BKS.Cg-Dock7^m +/+ *Lepr^{db}*/J, JAX#000642) and their corresponding control C57BLKS/J mice (JAX#000662) were obtained from the Jackson Laboratory (Sacramento, CA). To examine the effects of elevated ketone bodies in vivo, C57BLKS/J and db/db mice were randomly distributed in 4 groups. Two groups were subjected to a ketogenic diet containing 6% D- β -OHB-(R)-1,3 butanediol monoester (KE replacing equicaloric amounts of carbohydrate),³¹ and 2 other groups were fed control diet.

Animals were acclimated for 4 days before the experimental diets were started. Then, all mice were trained to eat the control liquid diet for 3 days, by placing feeding tubes with liquid diet in addition to chow, as shown in Figure 1A. After the training period, the chow was removed, and all groups were switched to the corresponding liquid diets. KE diet groups were initially fed a diet containing 3% (w/v) KE for 3 days. The KE concentration in the diet was increased to 4.5% w/v after 3 days and to 6% after 6 days. The 6% KE diet was used for the remainder of the study. KE groups were fed ad libitum. The control diet animals were pair-fed to the KE groups, in that the control group was given the average amount of liquid diet consumed by the KE group the day before. Feeding bottles with fresh food were provided every evening, \approx 30 minutes before the start of the dark cycle.

Diets and Preparations

Powdered Lieber-DeCarli diets were obtained from Bio-Serv (products F1258SP and F1259SP; Bio-Serv, Frenchtown, NJ). The liquid control diet was prepared by adding warm water to the Lieber-DeCarli control diet powder. The KE diet was prepared by adding warm water to the base of the ethanol diet F1258SP but instead of ethanol, KE was added as an equicaloric replacement for maltodextrin. The composition of each diet is listed in Table. The amount of fat, proteins, and total calories per gram was equal in both diets (control and KE).

Measurements of Blood Ketone and Glucose Levels

Nonfasting blood β -OHB and glucose levels were measured with commercially available colorimetric assays (Cayman Chemicals Kit #700190 for β -OHB and Sigma High Sensitivity Assay kit MAK181 for glucose) according to the manufacturer's instructions. During feeding experiments, nonfasting blood glucose and β -OHB levels were periodically checked with glucose

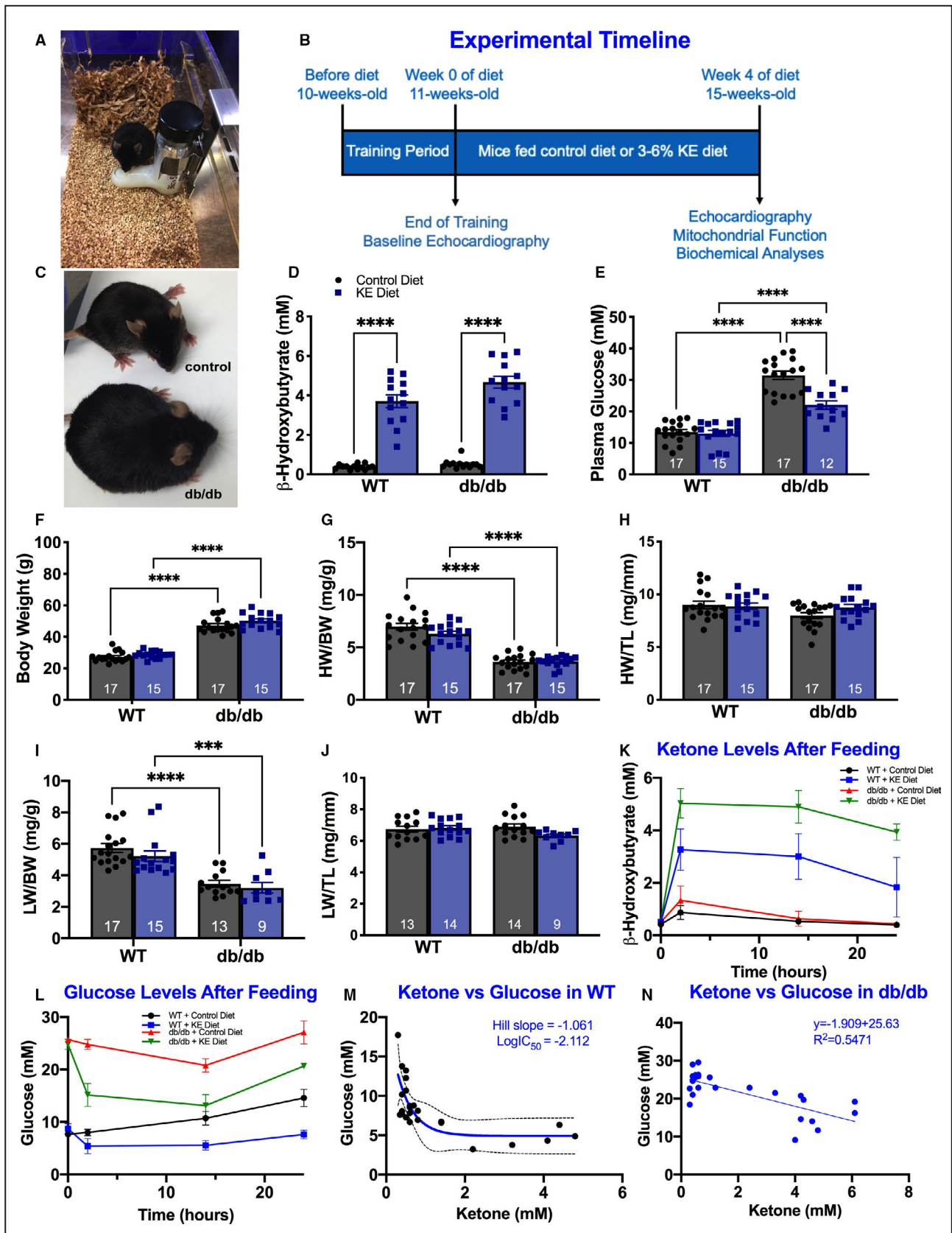


Figure 1. Effects of ketone ester diet on ketone levels, body weight, and glucose levels.

A, Image shows administration of liquid diet protocol. **B**, Experimental protocol for the study. **C**, Picture shows a representative image of WT mouse (top) and a mouse with type 2 diabetes mellitus (db/db, bottom). Summary data of **(D)** β-hydroxybutyrate and **(E)** plasma glucose taken at 4 weeks after administration of liquid diet. Morphometric parameters such as **(F)** body weight, **(G)** heart weight to body weight ratio, **(H)** heart weight to tibial length, **(I)** lung weight to body weight, **(J)** and lung weight to tibial length were taken at 4 weeks. After feeding, some mice underwent periodic ketone and glucose measurements. Summary data of **(K)** ketone levels after feeding, **(L)** glucose levels after feeding, **(M)** ketone levels vs glucose levels in WT, and **(N)** ketone levels vs glucose levels in db/db mice are shown. Data expressed as mean±SEM with n as the number of mice in the bar graphs. ****P*<0.001, and *****P*<0.0001 and it is calculated using 2-way ANOVA with Tukey’s post hoc multiple comparison. HW/BW (mg/g) indicates heart weight/body weight (mg/g); HW/TL (mg/mm), heart weight/tibial length; KE, ketone ester; and LW/TL (mg/mm), lungs weight/tibial length. LogIC50 is the log of the concentration of competitor that results in binding halfway between Bottom and Top. IC50 represents the concentration at which a substance exerts half of its maximal inhibitory effect.

and ketone sticks using a Precision Xtra meter (Abbott Laboratories, Abbott Park, IL).

Pulmonary congestion was examined by calculating lung weight-to-tibial length ratios.

Echocardiography

Cardiac function was examined using 2D echocardiography using a VisualSonics Vevo 2100 echocardiography machine (VisualSonics, Toronto, ON, Canada) and a MS 550D probe (22–55 MHz) under anesthesia with 1% to 1.5% isoflurane in a 100% O₂ atmosphere gas chamber. Some recordings were performed in conscious animals to exclude the effects of anesthesia on cardiac function (Figures S1 and S2). Fractional shortening, ejection fraction, stroke volume, and cardiac output were calculated from the M-mode images. Left ventricular (LV) mass was calculated using M-mode data as reported by Troy³⁷ using the following equation: LV mass (Troy) = 1.05 [(LVIDD+LVPWT+IVSD]³–[LVIDD]³), where LVIDD is LV internal diameter at diastole, LVPWT is LV posterior wall thickness at diastole and IVSD is intraventricular septum thickness at diastole.

Doppler imaging was performed to determine peak velocity during rapid filling phase in early diastole (E wave), and peak filling velocity in late diastole as a result of atrial contraction (A wave), and E/A ratios.

Morphometric Measurements

Four weeks after diet intervention, mice were anesthetized in a gas chamber with 3% to 5% isoflurane in a 100% O₂ atmosphere and euthanized. Each animal was euthanized by exsanguination under deep anesthesia. Hearts and lungs were excised, blotted dry, and weighed. Tibial length was measured with a Vernier caliper and used to normalize heart/lung weights. Increased cardiac mass was evaluated by examining the ratios between heart weight and tibial length.

Western Blotting

Hearts were homogenized in ice-cold RIPA lysis buffer, and protein content was measured using the Bicinchoninic Acid (BCA) Protein Assay. Blocked membranes were incubated with primary antibodies toward total β-hydroxybutyrate dehydrogenase (BDH1; Abcam ab193156), OXCT1 (SCOT; Abcam ab105320), and acetyl-CoA acetyltransferase 1 (ACAT1; Abcam ab168342). Membranes were scanned using the Licor Odyssey infrared imaging system and analyzed with ImageJ software. Band intensities of all samples were normalized to the internal housekeeping proteins (GAPDH; Abcam ab8245 or α-tubulin; Abcam ab7291) that were included on each gel.

Some experiments were performed using the Jess capillary western blot system according to the manufacturer specifications (Protein Simple, San Jose, CA). Briefly, tissue lysates were loaded in 24-well Protein Simple plates together with primary antibodies (Total OXPHOS Rodent WB Antibody Cocktail; Abcam ab110413) and outer mitochondrial membrane voltage-dependent anion channel 1 (Abcam; ab15895), secondary antibodies (anti-mouse near infrared and anti-rabbit horseradish peroxidase from Protein Simple), protein normalizing reagent, and chemiluminescent substrates. Proteins were separated within individual capillaries using Protein Simple cartridges. The signal intensity was analyzed as area under the curve for each protein peak using Protein Simple Software and normalized to total protein or loading control of interest. Digital images were generated for visual representation of the signal. For the antioxidant enzymes, primary antibodies against catalase (ab16731), thioredoxin (ab273877), superoxide dismutase 1 (SOD1; ab51254) and glutathione peroxidase 4 (GPX4; ab125066) were used. Data were normalized to GAPDH loading control (ab8245). For mitophagy experiments, primary antibodies against PTEN-induced putative kinase 1 (PINK1; Abcam ab23707), cytosolic E3 ubiquitin ligase (Parkin; Abcam ab15954), mitofusin 2 (Mfn2; ab124773), SQSTM1/p62 (The p62 protein is also called sequestosome 1) (Abcam ab56416), and microtubule-associated protein 1 light chain 3 (LC3; Abcam ab192890) were used. GAPDH (Abcam ab9483) was used as a loading control.

TABLE 1. Control and Ketone Ester Diets Composition

Diet composition	Control diet	KE diet
Protein content (kcal/L)	151	151
Fat content (kcal/L)	359	359
Carbohydrate content (kcal/L)	490	135
Ketone content (kcal/L)	0	355
Total (kcal/L)	1000	1000

Mitochondrial Respiratory Chain Coupling and Electron Flux

Mitochondria were isolated using a standard differential centrifugation method.⁵ Briefly, minced hearts were placed in mitochondrial isolation buffer 1 in 67 mM sucrose, 50 mM Tris/HCl, 50 mM KCl, 10 mM EDTA, and 0.2% BSA with a pH=7.2, homogenized with a glass Teflon pestle, and subsequently centrifuged at 700g for 10 minutes at 4 °C. The supernatant was collected and centrifuged at 8000g for 10 minutes at 4 °C. The pellet was then resuspended in ice-cold buffer (isolation buffer 2) containing 250 mM sucrose, 3 mM EGTA/Tris, and 10 mM Tris/HCl with a pH=7.2, followed by centrifugation at 8000g for 10 minutes at 4 °C. Mitochondria were then resuspended and stored in isolation buffer 2. Protein concentration was determined using the Bradford Assay. Coupling and electron flux assays were performed as described.³⁸

Cell Isolation

Hearts were excised from adult db/db and age- and strain-matched WT mice. Hearts were placed on a Langendorff-perfusion apparatus and perfused for 6 minutes at 37 °C with nominally Ca²⁺-free DMEM (GIBCO type 22 300) gassed with a 95% O₂/5% CO₂ mixture. Perfusion was then switched to the same solution containing Liberase TM (Research Grade, Roche) and 20 μmol/L Ca²⁺ with perfusion continuing until the heart became flaccid (≈7–12 minutes). Atria were removed, enzyme activity was blocked by switching the solution to DMEM containing 0.5% to 1% BSA, and the ventricles were cut into smaller pieces and gently pushed up and down with a plastic transfer pipette to separate individual cells. Isolated cells were kept in MEM solution with 50 μmol/L Ca²⁺ at room temperature (22–24 °C) until used for experimentation or placed in a short-term culture (see below). For confocal measurements, isolated cardiomyocytes were plated on glass coverslips with laminin coating. All experiments were performed at room temperature (22–24 °C).

Mitochondrial Membrane Potential Measurements

Mitochondrial membrane potential ($\Delta\Psi_m$) was measured in intact freshly isolated cardiomyocytes using the potentiometric probe tetramethylrhodamine methyl-ester (λ_{ex} =543 nm and λ_{em} =565–605 nm).^{39–42}

Mitochondrial Permeability Transition Pore Activity

Mitochondrial permeability transition pore (mPTP) activity was measured in permeabilized cells incubated with 5 μM calcein/AM (λ_{ex} =488 nm, λ_{em} =510 nm) for 40 minutes at 37 °C.^{39,43–45} Opening of mPTP induces the loss of mitochondria-trapped calcein (620 Da) and

a decrease of fluorescence. At the end of each recording 10 μg/mL of the pore-forming antibiotic alamethicin was added to obtain a maximum calcein release from mitochondria for data normalization.

Oxidative Stress and Redox Measurements in Cultured Cardiomyocytes

To examine oxidative stress in db/db and corresponding control cardiomyocytes, we employed adenoviral construct to express redox-sensitive green fluorescent protein 2 (roGFP2) fused to specific sensor domains to measure changes in H₂O₂ either in mitochondria or cytosol of intact cells.^{27,46} For this sensor to be specific for H₂O₂, the redox-sensitive roGFP2 was fused with the yeast peroxidase ORP1.⁴⁷ When ORP1 reacts with H₂O₂, it forms a cysteine sulfenic acid in the active site, leading to the formation of protein disulfide bonds in roGFP2, thus shifting the 405/488-nm excitation ratio.⁴⁷

To monitor redox changes inside the cytosol and mitochondria, a fusion construct roGFP2-GRX1 was employed. roGFP2-GRX1 uses human glutaredoxin to sense the changes in oxidized glutathione (GSSG) relative to the level of reduced glutathione (GSH).^{48–50} To calibrate the signal, diamide was added at the end of each experiment to oxidize the GSH pool and obtain R_{max} for the roGFP2 probe and DTT to obtain R_{min} . Mitochondrial targeting of both constructs was obtained by fusion of roGFP2-ORP1/roGFP2-GRX1 to the mitochondrial targeting sequence of the first 69 amino acids of subunit 9 of the F₀-ATPase of *Neurospora crassa*.⁵¹ Both constructs were excited with the 405- and 488-nm laser lines, and emission was detected at 510 nm. These 2 excitation peaks have different redox dependence where cysteine oxidation induces increase in 405-nm excitation peak and a corresponding decrease in 488-nm excitation peak, while cysteine reduction has an inverse effect. Therefore, the ratio in emission recorded at 405- to 488-nm excitation wavelengths is used as a measure of the relative amount of oxidized to reduced roGFP2.^{49,50}

To express these adenoviral constructs, freshly isolated cardiomyocytes were placed in a short-term (24–48 hour) culture in MEM (Invitrogen) supplemented with 2 mM glutamine, 1X insulin (1 mg/mL)-transferrin (0.55 mg/mL)-selenium (0.67 ng/mL), 0.2% bovine serum albumin, 4 mM NaHCO₃, 10 mM HEPES, 100 U/mL penicillin-streptomycin, and 25 μM Blebbistatin. 2 mM β-OHB was added to the medium of KE-treated groups to maintain the elevated β-OHB concentration during cell culture.

Mitochondrial Redox State

Flavin adenine dinucleotide (FAD)-linked protein auto-fluorescence (λ_{ex} = 488 nm, λ_{em} = 510 nm) was used as another measure of the mitochondrial redox state in

freshly isolated cardiomyocytes.⁴⁴ Data are presented as the ratio of oxidized FAD to reduced FADH₂ (FAD/FADH₂) calculated as $(F - F_{\min}) / (F_{\max} - F_{\min})$ where F is the fluorescence intensity recorded from the mitochondrial regions of interest. F_{min} is the fluorescence obtained after addition of 4 mM NaCN (inhibits respiration and promotes maximal FAD reduction, ie, FADH₂ formation), taken as 0%. F_{max} is the fluorescence obtained after addition of 4 μM carbonyl cyanide 4-(trifluoromethoxy)-phenylhydrazone (FCCP) (stimulates maximal respiration, completely oxidizing the mitochondrial FADH₂ pool), taken as 100%.

Mitophagy Markers Measurements

To measure Parkin accumulation in mitochondria and LC3-mediated autophagosome formation, mCherry-Parkin and GFP-LC3 were expressed in cardiomyocytes via adenoviral gene transfer as previously described.^{27,52} Culturing conditions were the same as described above for redox sensitive constructs. mCherry-Parkin fluorescence was excited at 540 nm and monitored at 590 nm while GFP-LC3 fluorescence was measured with $\lambda_{\text{ex}}=488$ nm and $\lambda_{\text{em}}=510$ nm.

Statistical Analysis

All data were analyzed using unpaired t-tests or two-way ANOVA with Bonferroni's post-hoc, using Prism version 7.0 (Graph-Pad Software Inc., San Diego, CA), and $P < 0.05$ was considered statistically significant. All data are shown as mean \pm SEM. The complete list of P values is listed in S1.

RESULTS

Effects of KE Diet on Ketone Levels, Body Weight, and Glucose Levels

The compositions of the control and KE diet are reported in Table. As shown in the experimental protocol (Figure 1B), mice underwent a training period for acclimation, followed by 4 weeks of dietary intervention. At this age (11 weeks), T2DM mice were already significantly overweight (Figure 1C). After 4 weeks of diet intervention, both WT (4.04 ± 0.29 versus 0.31 ± 0.04 mM; $P < 0.05$) and db/db mice (4.36 ± 0.32 versus 0.45 ± 0.08 mM; $P < 0.05$) fed the KE diet showed a significant increase in circulating β -OHB levels as compared with mice on control diet (Figure 1D). This shift in energy substrate in the blood corresponded with a concomitant decrease in glucose concentration in db/db mice (Figure 1E). WT control mice had a glucose concentration of 13.4 ± 0.7 mM ($n=17$), which was not different from WT fed the KE diet (13.04 ± 0.9 mM, $n=15$). Glucose concentration was elevated in db/db mice (31.5 ± 1.3 mM, $n=17$), but this increase was

significantly less pronounced in db/db mice fed the KE diet (21.7 ± 1.1 mM, $P < 0.05$, $n=15$).

Diabetic mice on control diet showed significantly increased body weights compared with their control WT (47.21 ± 1.33 versus 27.3 ± 0.78 g; $n=17$ for both groups; $P < 0.05$; Figure 1F). Heart weight, when normalized to body weight, was significantly reduced in diabetic mice compared with WT groups (Figure 1G); however, no difference was observed in heart weight normalized to tibial length in db/db mice fed the control diet relative to WT control mice even though there was a trend to decline (7.99 ± 0.36 versus 8.99 ± 0.36 mg/mm; $P=0.09$; Figure 1H). Similarly, we did not observe significant differences in the lung weight normalized to tibial length (6.98 ± 0.19 versus 6.74 ± 0.15 mg/mm; $n=14$; $P=0.9$) between db/db and WT groups on control diet (Figure 1J), but the lung weight normalized to body weight was significantly decreased in db/db mice (Figure 1I). A KE diet did not affect heart or lung weight in both control and diabetic animals.

In a separate experiment, we monitored changes in circulating β -OHB and glucose levels 2, 14 and 24 hours after feeding. We detected a significant increase in β -OHB 2 hours after feeding, which steadily decreased over the time but still remained elevated even 24 hours after the feeding (Figure 1K). Together with the increase in circulating β -OHB, we observed a decrease in glucose concentration in KE-fed mice (Figure 1L). When we plotted the glucose concentration versus circulating ketone levels in WT (Figure 1M) and db/db mice (Figure 1N), we discovered an inverse linear relationship between ketone levels and glucose concentration in diabetic hearts; however, an inverse sigmoidal relation was noted between ketone and glucose levels in WT mice.

In summary, these data demonstrate that KE supplementation led to a significant increase in circulating β -OHB in both control and db/db mice that was associated with a decline in circulating glucose levels. However, without calorie restriction, db/db mice on the KE diet did not lose any weight as compared with the db/db mice on the control diet.

KE Diet Improves Cardiac Function in Mice With T2DM

Echocardiography was used to determine the effects of dietary intervention on cardiac structure and function. B-mode videos taken at the parasternal long-axis view (Figure 2A) were used to acquire the width (Figure 2B) and length (Figure 2C) of the left ventricle, and videos taken at the parasternal short axis view were used to acquire endocardial area of the hearts at diastole. We did not detect a significant difference in terms of the width and length of the hearts, but

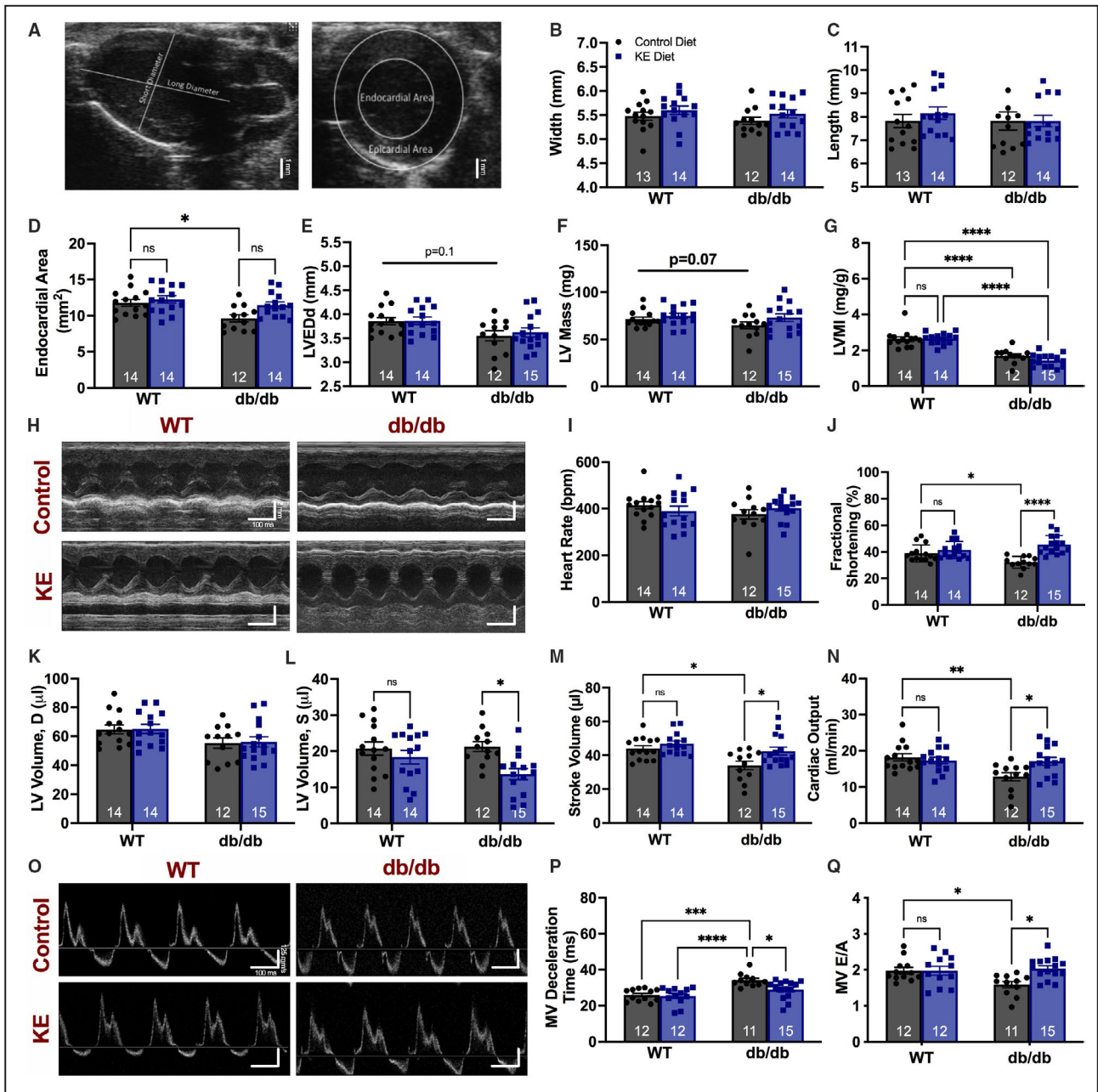


Figure 2. Ketone ester diet improves cardiac function in mice with type 2 diabetes mellitus.

Systolic function, diastolic function, and cardiac dimensions were assessed using echocardiography. **A**, Representative parasternal long-axis and parasternal short-axis M-modes are shown. Summary data of cardiac dimensions of **(B)** width, **(C)** length, **(D)** endocardial area, **(E)** left ventricular end diastolic diameter at diastole (LVEDd), **(F)** left ventricular mass corrected, and **(G)** left ventricular mass index (LVMI) are shown. Panel **(H)** displays representative M-mode images. Time bar, 100 msec. Scale bar, 22 mm. Summary data of **(I)** heart rate, **(J)** fractional shortening, **(K)** left ventricular volume at diastole, **(L)** left ventricular volume at systole, **(M)** stroke volume, **(N)** and cardiac output are shown. Panel **(O)** shows representative images of pulse-wave doppler of blood velocity profiles of all four groups. Time bar, 100 msec. Velocity scale bar, 125 mm/sec. Summary data of **(P)** mitral valve deceleration time and **(Q)** mitral valve E to A ratio are shown. Data expressed as mean±SEM with n as the number of mice in the bar graphs. **P*<0.05, ***P*<0.01, ****P*<0.001, and *****P*<0.0001, and it is calculated using 2-way ANOVA with Tukey’s post hoc multiple comparison. AW indicates left ventricular anterior wall; db/db indicates type 2 diabetic mice; KE Diet, ketone ester diet; LV Mass AW (mg), left ventricular mass (mg); MV Deceleration Time (ms), mitral valve deceleration time (ms); MV E/A, mitral valve E/A ratio where E wave is the peak velocity during rapid filling phase in early diastole, and A wave is the peak filling velocity in late diastole as a result of atrial contraction; and WT, wild type.

we found that endocardial area (Figure 2D) was significantly smaller in db/db control mice relative to WT control mice (*P*<0.05). Although not significant, the LV

end-diastolic diameter (Figure 2E) as well as the corrected LV mass (Figure 2F) were lower in db/db control mice versus WT control mice and were normalized in

mice fed a KE diet. Indeed, and as expected, when the LV mass was normalized to body weight, we saw a significant difference in db/db mice relative to their respective controls (Figure 2G).

While the KE diet modestly affected cardiac structure, we found that cardiac function was significantly improved, as depicted by the representative M-mode images that show more robust contraction (Figure 2H). During the imaging procedure, mice were lightly anesthetized with 0.75% to 1% isoflurane, which did not differentially affect their heart rates (Figure 2I). Although the KE diet did not affect the cardiac function of WT mice, it did significantly affect the systolic function of db/db mice. As evidenced in Figure 2J, fractional shortening was significantly lower in db/db control mice versus WT control mice ($39\pm 2\%$ versus $32\pm 1\%$; $P<0.05$). Db/db mice fed a KE diet exhibited more robust fractional shortening as compared with db/db mice fed a control diet ($45\pm 2\%$ versus $32\pm 1\%$; $P<0.0001$). This is reflected also in the LV volume at diastole (Figure 2K) and LV volume at systole (Figure 2L). Although there was no difference in LV volume at diastole between the db/db groups, LV volume at diastole was significantly lower in db/db mice on a KE diet relative to db/db mice on a control diet, suggesting that more volume was ejected from the left ventricle during contraction. Indeed, since heart rate was maintained at the same level, stroke volume (Figure 2M) and, therefore, cardiac output (Figure 2N) were significantly lower in db/db control mice relative to db/db KE mice. To rule out the effects of anesthesia on systolic function, we performed echocardiography in conscious mice (Figure S1). Consistent with our echoes in sedated animals, we found that db/db mice fed a KE diet exhibited significantly greater systolic function relative to db/db mice fed a control diet.

Diastolic function was assessed using pulse-wave Doppler at the mitral valve (MV). We calculated the ratio between peak blood flow velocity during early diastole, E wave, and peak flow velocity during atrial contraction, A wave, as well as examined the MV deceleration time to assess diastolic function. Representative images of wave blood flow profiles are depicted in Figure 2O. The MV deceleration time (Figure 2P) was significantly prolonged in db/db mice on a control diet relative to WT mice on a control diet (34.2 ± 1.1 versus 25.9 ± 1.0 ms; $P<0.001$). KE diet did not affect MV deceleration time in WT mice. However, it significantly improved MV deceleration time in db/db mice ($P<0.05$). Additionally, the E/A ratio (Figure 2Q) was significantly lower in db/db mice on a control diet compared with WT mice on a control diet (1.59 ± 0.09 versus 1.98 ± 0.09 , $P<0.05$). Db/db mice fed a KE diet exhibited a more normalized MV E/A ratio relative to db/db mice fed a control diet (2.03 ± 0.08 versus 1.59 ± 0.09 ; $P<0.05$). Taken together,

while the KE diet modestly affected cardiac structure, it significantly improved systolic and diastolic function in db/db mice.

KE Diet Increases Expression Level of Key Ketolytic Enzymes

After 4 weeks of feeding, hearts were collected and protein lysates were prepared to determine protein expression level of key ketolytic enzymes: BDH1, SCOT, and mitochondrial ACAT1. The schematic representation of the ketogenic pathway in the heart is illustrated in Figure 3A with representative blots of BDH1, SCOT, and ACAT1 shown in Figure 3B. In cardiomyocytes, BDH1 catalyzes the reaction of β -hydroxybutyrate to acetoacetate; SCOT catalyzes the reaction of acetoacetate to acetoacetyl-CoA; and ACAT1 catalyzes the reaction of acetoacetyl-CoA to 2 acetyl-CoAs. These acetyl-CoAs then feed into the TCA to produce high-energy electron carriers. There was a significant down-regulation in BDH1 expression in db/db mice on the control diet compared with the WT mice on the control diet ($P<0.05$). KE diet restored BDH1 expression levels in db/db mice back to those of WT (Figure 3C). However, there was a significant increase in SCOT expression in WT KE mice and db/db KE mice, relative to the corresponding control diet mice ($P<0.05$; Figure 3D). Furthermore, ACAT1 was elevated in KE-fed db/db mice compared with db/db mice on the control diet ($P<0.05$; Figure 3E). These data demonstrate that the KE supplementation induced almost a 2-fold increase in SCOT expression in both WT and T2DM hearts and 25% increase in ACAT1 expression only in diabetic hearts, which would be predicted to increase β -OHB metabolism and fuel delivery to the TCA cycle.

Ketone Ester Diet Enhances Basal and ADP-Dependent Oxygen Consumption Rates in Both WT and db/db Hearts

To determine if the increase in ketone levels altered mitochondrial respiration, we isolated mitochondria from all four groups and measured the oxygen consumption rate (OCR) using a Seahorse Bioscience Extracellular Flux XF24 Analyzer. Ten micrograms of mitochondrial protein was loaded in each experimental well except background wells, and all data are presented as OCR per 10 μ g of mitochondrial protein.

First, we designed Seahorse experiments in a manner which allows to measure OCR in mitochondria under conditions which support oxygen consumption at the level of mitochondrial complex I (10 mM Pyruvate and 2 mM Malate), complex II (10 mM Succinate after complex I inhibition with Rotenone), and complex IV (100 μ M N,N,N',N'-Tetramethyl-p-phenylenediamine dihydrochloride (TMPD) with 10 mM ascorbate) after

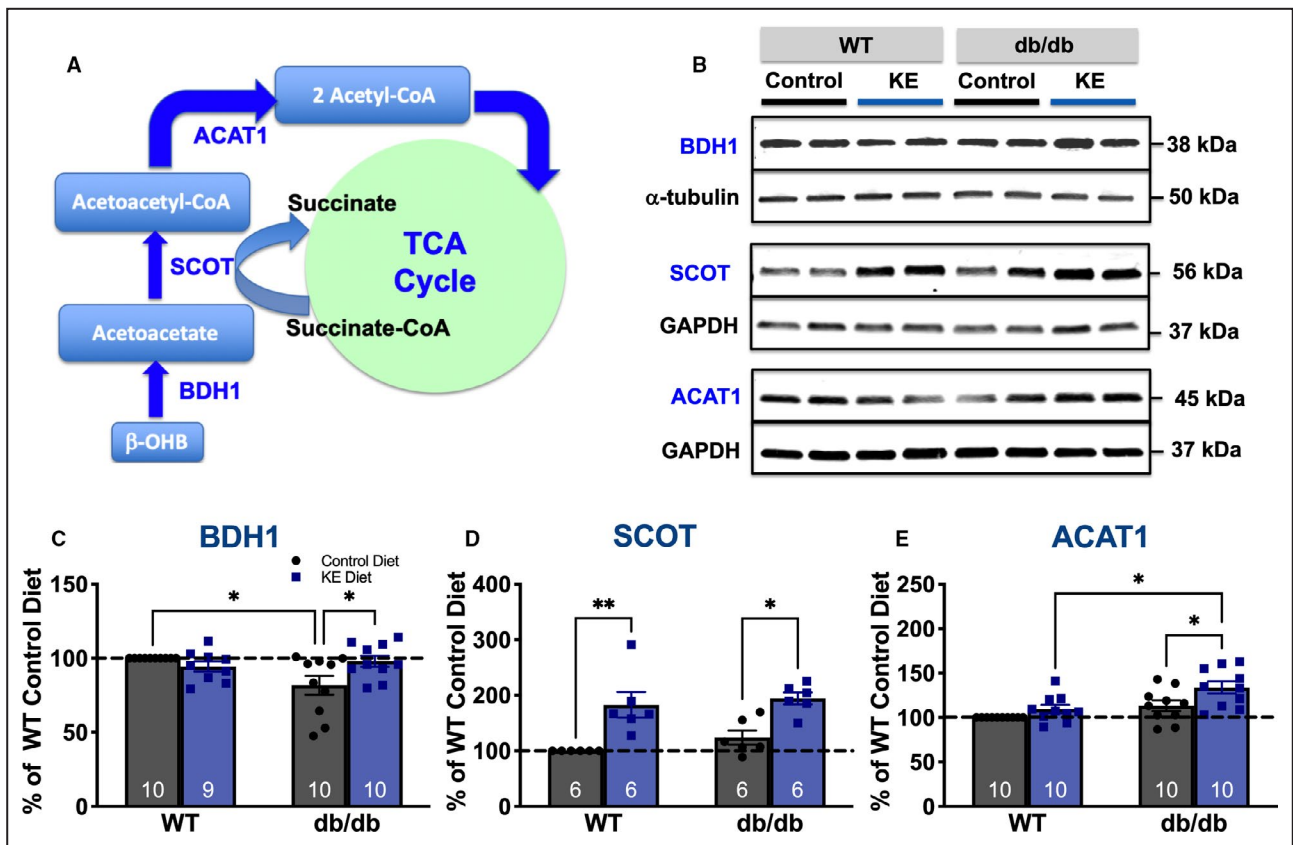


Figure 3. Ketone ester diet increased expression level of key ketogenic enzymes.

After 4 weeks of feeding, tissue protein lysates were prepared to measure protein expression level of key ketogenic enzymes. **A**, A schematic representation of ketogenic pathway in the heart is shown. **B**, Representative blots of mitochondrial β -hydroxybutyrate dehydrogenase (BDH1), succinyl-CoA:3-ketoacid transferase (SCOT), and mitochondrial acetyl-CoA acetyltransferase 1 (ACAT1) are shown. Summary data of **(C)** BDH1, **(D)** SCOT, and **(E)** ACAT1 are displayed. Data expressed as mean \pm SEM with n as the number of samples in the bar graphs. * P <0.05, ** P <0.01, *** P <0.001, and **** P <0.0001, and it is calculated using 2-way ANOVA with Tukey's post hoc multiple comparison. Dashed line represents the basal level of protein expression in wild-type (WT) animals fed a control diet. This level was set as 100% and used for normalization of protein expression in WT animals treated with ketone ester (KE) and in diabetic animals treated with control and KE diet.

complex III activity was inhibited with 4 μ M antimycin A. These experiments were performed under uncoupling conditions (ie, in the presence of 4 μ M FCCP). Figures 4A and 4B show that mitochondrial complex I activity was significantly higher in db/db mice (red) on control diet as compared with their corresponding WT mice on control diet (black). A KE diet significantly increased complex I activity in WT (blue) to the level recorded in db/db mice on control diet. However, the highest OCR was observed in mitochondria from db/db mice on KE diet (green). Mitochondrial complex I activity was then inhibited by addition of 2 μ M rotenone, and 10 mM succinate was supplied to activate mitochondrial complex II. Similarly, complex II activity was higher in db/db versus WT mitochondria on the control diet, and the KE diet further enhanced complex II OCR in both WT and db/db mitochondria. Next, 4 μ M antimycin A was injected to block complex III activity, and then 100 μ M TMPD with 10 mM ascorbate were

added to stimulate complex IV. As for Complex I and II, Figures 4C and 4D show that the activity of complex IV was similarly increased in db/db versus WT mice and further improved with the KE diet in both groups. These data indicate that KE increased OCR in both WT and db/db mitochondria.

Next, we performed mitochondrial coupling assays (Figure 4C and 4D), where mitochondria were placed in the respiration medium containing 10 mM succinate and 2 μ M rotenone, reflecting complex II-mediated oxygen consumption. Then, 4 mM ADP (state 3), 2.5 μ g/mL oligomycin (state 4_o), and 4 μ M FCCP (state 3_u), and 4 μ M antimycin A were sequentially injected into the wells (Figure 4C). We found that, similar to results shown in Figures 4A and 4B, basal mitochondrial OCR upon activation of mitochondrial complex II was significantly elevated in the WT KE-fed mice (717 \pm 41 pmole/min, P <0.0001) and db/db KE-fed mice (925 \pm 43 pmoles/min; P <0.05) as compared

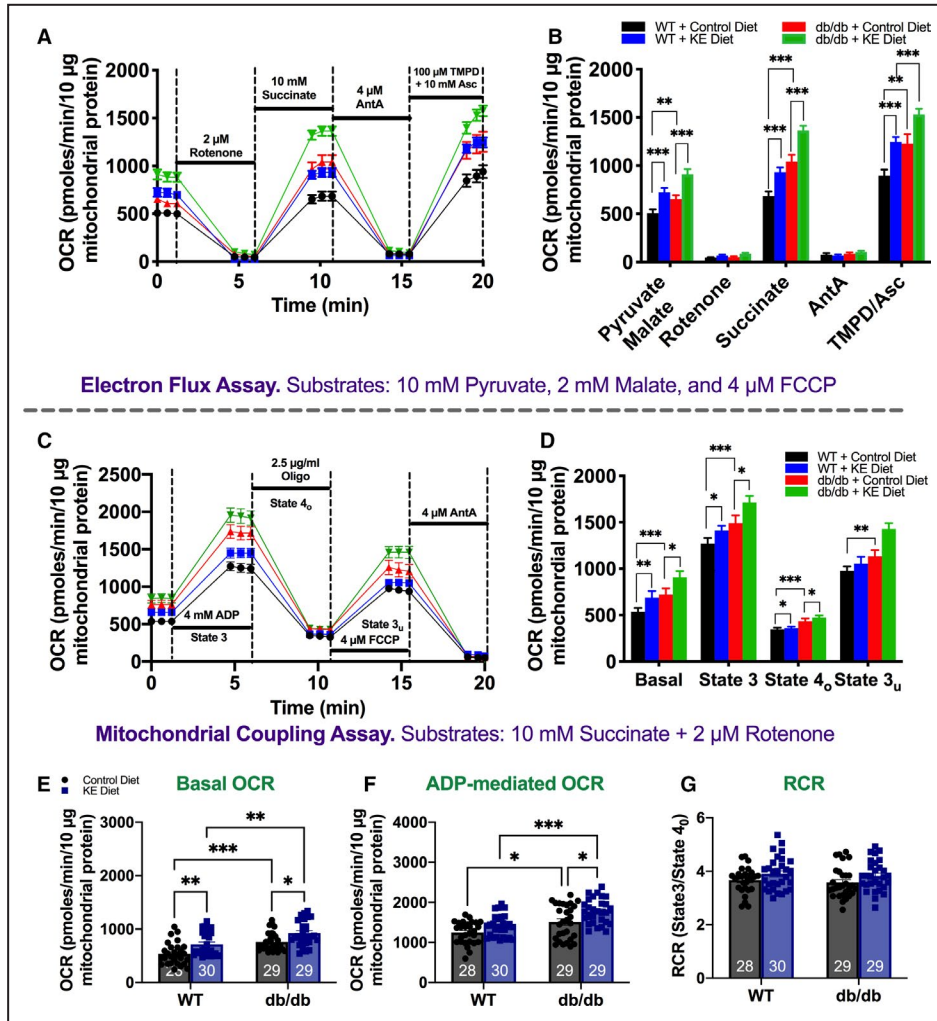


Figure 4. Ketone ester diet enhances basal oxygen consumption rates and induces mild uncoupling in both wild-type (WT) and type 2 diabetic (db/db) hearts.

Dashed line is used to separate 2 types of experiments: The top summarizes the electron flow assay data and the bottom summarizes data for the mitochondrial coupling assay. **A**, Representative traces of mitochondrial oxygen consumption rate (OCR) in freshly isolated heart mitochondria from WT and db/db mice under basal conditions (10 mM pyruvate, 2 mM malate, and 4 µM FCCP), after 2 µM rotenone, 10 mM succinate, 4 µM antimycin A, and 100 µM TMPD plus 10 mM Ascorbate application are shown. **B**, Summary of the electron flux assay parameters in cardiac mitochondria from WT and diabetic mice fed either a control or KE diet. **C**, Representative traces of the mitochondrial oxygen consumption rate (OCR) in freshly isolated cardiac mitochondria from WT and db/db mice under basal conditions (10 mM succinate and 2 µM rotenone), after 4 mM ADP, 2.5 µg/mL oligomycin, 4 µM FCCP, and 4 µM antimycin A application are shown. **D**, Summary of the OCR under coupling and uncoupling conditions in cardiac mitochondria from WT and diabetic mice fed either a control or KE diet. **E**, Summary of the basal OCR in cardiac mitochondria from WT and diabetic mice fed either a control or KE diet. **F**, Summary of ADP-induced OCR in cardiac mitochondria from WT and diabetic mice fed either a control or KE diet. **G**, Summary of the mitochondrial coupling calculated as State 3/State_{4o} ratio in cardiac mitochondria from WT and diabetic mice fed either a control or KE diet. Summary data reflect the mean of 28–30 measurements per group in isolated mitochondria from 4 different animals. Data expressed as mean±SEM. **P*<0.05, ***P*<0.01, and ****P*<0.001 and it is calculated using two-way analysis of variance (ANOVA) with Tukey’s post hoc multiple comparison.

with WT control-fed mice (537±39 pmole/min) and db/db control-fed mice (761±33 pmole/min; *P*<0.001). Furthermore, basal OCR was significantly elevated in db/db mice on the control diet versus WT mice on

the control diet (Figure 4E). After the addition of ADP, the OCR of mitochondria from WT control-fed mice reached 1250±53 pmole/min, n=28 (state 3). State 3 of respiration was significantly higher in mitochondria

from db/db control-fed mice (1512 ± 78 pmole/min, $n=29$; $P<0.001$) compared with WT mice on the control diet, and in both KE groups (WT+KE= 1418 ± 46 pmole/min, $n=30$; and db/db+KE= 1777 ± 58 pmole/min, $n=28$) compared with their corresponding control diet groups ($P<0.05$) (Figure 4C and 4F). State 4_o was mediated through the addition of $2.5 \mu\text{g/mL}$ oligomycin that inhibits ATP synthase. After oligomycin addition, OCR decreased in all groups, but OCR was maintained at higher levels in mitochondria from db/db mice (both on control and KE diet), as compared with OCR of mitochondria from WT mice fed the control diet ($P<0.05$). Uncoupled oxygen consumption (state 3_u) achieved after addition of $4 \mu\text{M}$ FCCP was not different between WT and WT+KE mice; however, it was increased in db/db versus WT mice on the control diet ($P<0.001$), and further increased by the KE diet in db/db mice.

Finally, the mitochondrial complex III inhibitor, antimycin A, stops mitochondrial respiration in all 4 groups. The OCR levels obtained after antimycin A addition were subtracted from all measured OCR levels, and the corrected levels are presented in Figure 4D and 4G. Calculation of respiratory control ratio (state 3 /state 4_o) did not reveal any differences between WT (3.67 ± 0.09 ; $n=28$) and db/db mice (3.58 ± 0.11 ; $n=29$; $P=0.28$) fed control diet; or between WT+KE (4.06 ± 0.15 ; $n=30$) and db/db+KE (3.85 ± 0.11 ; $n=28$; $P=0.06$) mice as compared with their corresponding groups on the control diet (Figure 4G). Our respiratory control ratio obtained in cardiac mitochondria respiring on succinate are within the range or even higher compared with those reported by other labs.⁵³ This demonstrates a strong coupling between mitochondrial respiration and phosphorylation in our mitochondrial preparation. Furthermore, mitochondrial coupling was verified with a Clark-type electrode (Figure S3).

Based on these data, we concluded that neither mitochondrial respiratory flux nor coupling were compromised in mitochondria from T2DM mice (Figures 4C and 4G). Moderate elevation in β -OHB levels via KE supplementation increased basal and ADP-mediated oxygen consumption rates but did not increase the respiratory control ratio in either WT or T2DM mice (Figure 4G). To examine whether KE effects on both basal and ADP-induced oxygen consumption were mediated via an increase in mitochondrial biogenesis, we examined the expression of 3 proteins of the mitochondrial respiratory chain: (1) 30-kDa nuclear encoded subunit B of mitochondrial complex II, also known as succinate dehydrogenase (SDHB); (2) 40-kDa mitochondrially encoded subunit 1 of the mitochondrial complex IV, also known as cytochrome c oxidase I; and (3) 55-kDa mitochondrially encoded ATP synthase F1 subunit alpha. As shown in Figure 5, we did not observe a decline in expression of these proteins in db/db mice on the control

diet; however, there was a significant increase in expression of SDHB, cytochrome c oxidase I, and ATP synthase F1 subunit alpha in db/db mice fed the KE diet. Data were normalized either to total protein in panels 5B-D or mitochondrial loading control voltage-dependent anion channel 1) in panels 5E-G and are presented as a percent expression increase over WT mice on the control diet. We found that the expression of SDHB was increased by 30% to 40% relative to the WT on control diet ($n=6$ hearts), and the expression of cytochrome c oxidase I and ATP synthase F1 subunit alpha was increased by $\approx 30\%$ to 50% and 14% to 30% ($n=6$ hearts; $P<0.05$), depending on the normalization method. There was a significant increase in cytochrome c oxidase I expression in WT mice on the KE diet (+24% of WT+control diet), but there were no changes in SDHB or ATP synthase F1 subunit alpha expression. These data indicate that KE induces an increase in mitochondrial biogenesis in diabetic hearts and to a lesser degree in WT hearts.

KE Diet Decreases Reactive Oxygen Species Generation in Diabetic Mitochondria and Enhances Resistance to Oxidative Stress

Using a novel genetically encoded oxidative stress roGFP2-ORP1 sensor targeted to mitochondrial or cytosolic compartments,²⁷ we investigated the effects of the KE diet on oxidative stress in all 4 groups. Figure 6A shows representative images of WT control myocytes expressing the genetically encoded oxidative stress sensor cyto-roGFP2-ORP1 upon excitation at 488 nm (left panel) and 405 nm (middle panel). The right panel shows the overlay of both signals upon emission at 535 nm. These 2 excitation peaks have different redox dependence, where ORP1 oxidation induces an increase in the 405 nm excitation peak and a corresponding decrease in the 488 nm excitation peak, thereby increasing the 405/488 ratio.⁴⁷

The upper panels in Figure 6B validate the proper targeting of cyto-roGRP2-ORP1 construct to the cytosol (left panel) or mito-roGRP2-ORP1 to the mitochondrial compartment (right panel). In this case, after expression of either cyto-roGRP2-ORP1 or mito-roGRP2-ORP1, cells were loaded with 5 nM tetramethylrhodamine methylester to stain mitochondria (middle panels), and the correct targeting of the oxidative stress sensitive constructs was confirmed in the merged (low panels) images. As shown in the right panels, the signal recorded at 488 nm excitation for mitochondrially targeted construct almost completely overlapped with tetramethylrhodamine methylester signal, while the signal of cyto-roGRP2-ORP1 was primarily located at the cytosol. After proper conditions for expression were established, we expressed these

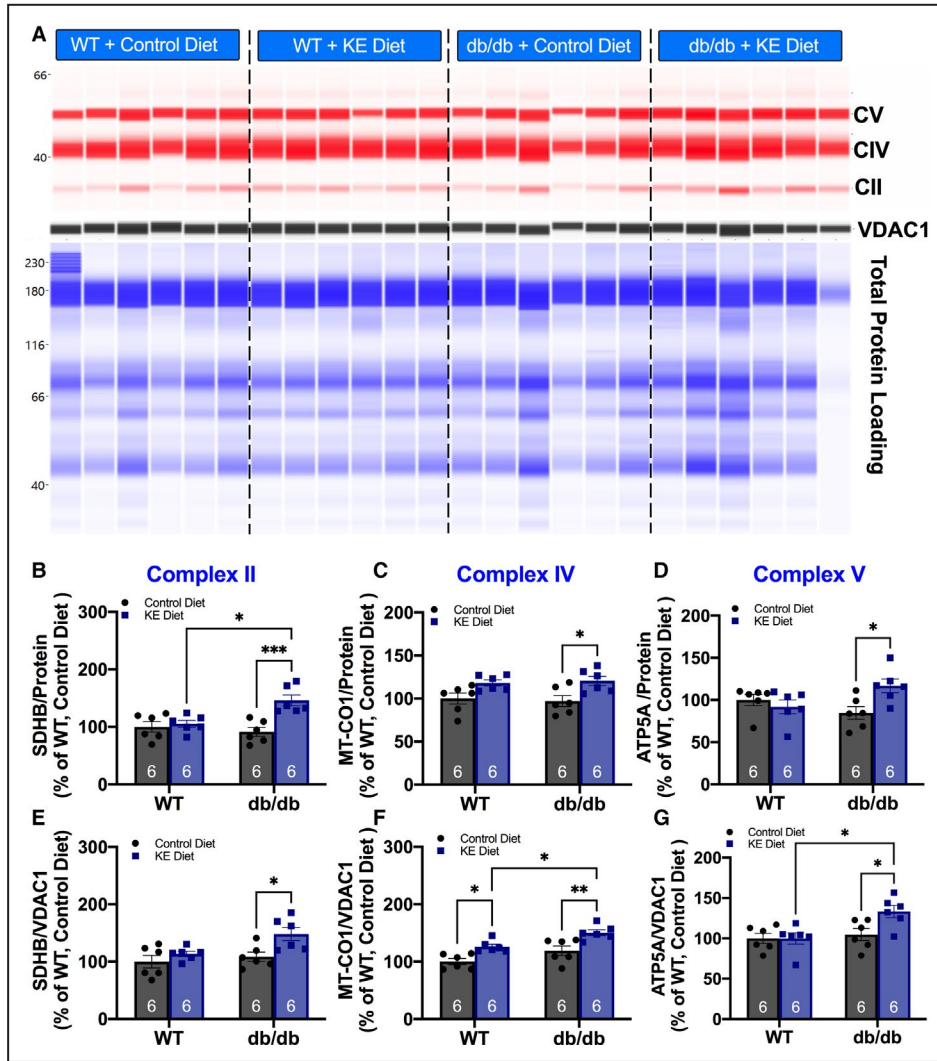
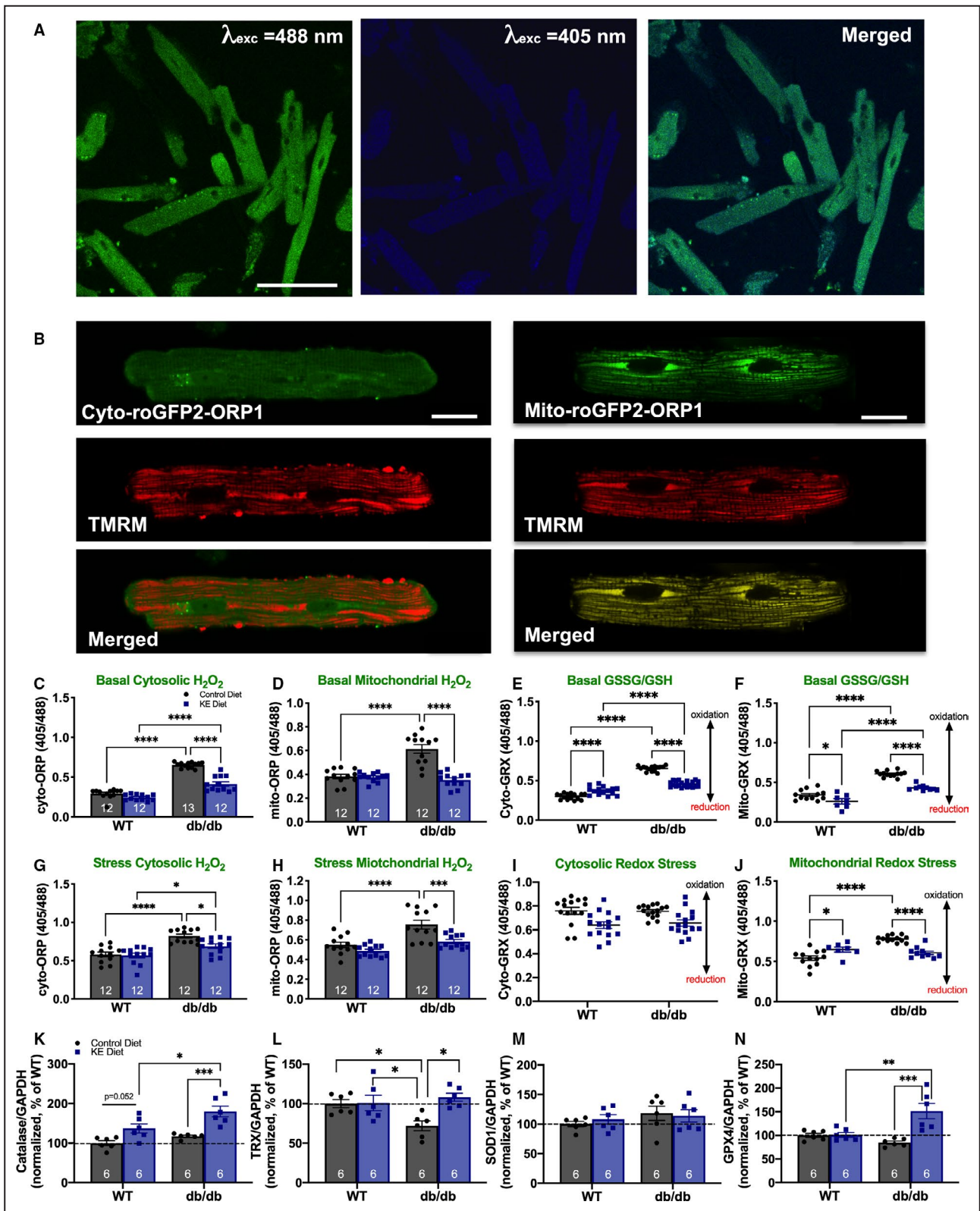


Figure 5. KE diet increases mitochondrial biogenesis in diabetic hearts.

A, Shown in red are the representative images of protein expression of 30-kDa nuclear encoded subunit B of the mitochondrial complex II (SDHB), 40-kDa mitochondrially-encoded subunit 1 of the mitochondrial complex IV (MT-CO1), and 55-kDa mitochondrially-encoded ATP synthase F1 subunit alpha (ATP5A) stained with secondary anti-NIR fluorescent antibodies. Shown in black are blots for the outer mitochondrial membrane voltage-dependent anion channel 1 (VDAC1) loading control detected with anti-rabbit HRP secondary antibodies. Total protein loading is shown in blue. **B-D**, Summary data of SDHB, MT-CO1 and ATP5A expression in cardiac mitochondria normalized to total protein loading from wild-type (WT) and diabetic mice fed either a control or KE diet are displayed. **E-G**, Summary data of SDHB, MT-CO1 and ATP5A expression in cardiac mitochondria normalized to VDAC1 from WT and diabetic mice fed either a control or KE diet are shown. Data are shown as a percent of WT+Control Diet Group taken as 100%. Data expressed as mean±SEM with n as the number of samples in the bar graphs. **P*<0.05, ***P*<0.01, and ****P*<0.001 and it is calculated using two-way analysis of variance (ANOVA) with Tukey’s post hoc multiple comparison.

constructs in cardiac myocytes from the 4 experimental groups and then measured basal levels of oxidative stress. As shown in Figures 6C and 6D, the basal level of oxidative stress was significantly elevated in cardiomyocytes isolated from db/db versus WT mice on the control diet in both the cytosolic and mitochondrial compartments (*P*<0.0001). In db/db myocytes, the KE

diet reduced H₂O₂ levels in both cytosolic (Figure 6C) and mitochondrial compartments (Figure 6D) as compared with myocytes from db/db mice on the control diet (*P*<0.0001). Furthermore, we used the genetically encoded redox sensor roGFP2-GRX1 to monitor redox changes inside the cytosol and mitochondria. roGFP2-GRX1 uses human glutaredoxin to sense the



changes in GSSG relative to the level of GSH.^{48–50} As shown in Figures 6E and 6F, both the cytosolic and mitochondrial basal redox state (ie, GSSG/GSH ratio) was shifted toward the oxidative state ($P < 0.0001$),

indicating depletion of the reduced glutathione pool. The KE diet prevented the depletion of the reduced glutathione pools in both cytosolic and mitochondrial compartments ($P < 0.0001$).

Figure 6. KE diet decreased reactive oxygen species generation in diabetic mitochondria and enhanced resistance to the oxidative stress.

A, Representative images of wild-type (WT) cardiomyocytes on control diet expressing a genetically-encoded oxidative stress sensor cyto-roGFP2-ORP1 upon excitation at 405 nm (left panel), 488 nm (middle panel), and overlay of both channels (right panel). **B**, Representative images of WT control cardiomyocytes expressing a genetically-encoded oxidative stress sensor roGFP2-ORP1 in cytosol (left panels) or mitochondria (right panels) upon excitation at 488 nm (upper panel) and co-loaded with membrane potential sensitive dye tetramethylrhodamine methylester (TMRM; middle), and overlay of both channels (low panels). Quantification of **(C)** basal cytosolic H_2O_2 , **(D)** basal mitochondrial H_2O_2 , **(E)** basal cytosolic GSSG/GSH, **(F)** basal mitochondrial GSSG/GSH signal, **(G)** stress-induced cytosolic H_2O_2 , **(H)** stress-induced mitochondrial H_2O_2 , **(I)** stress-induced cytosolic redox state, and **(J)** stress-induced mitochondrial redox state in cardiomyocytes from WT and db/db mice on control and KE diet. Summary data in each panel were calculated as average fluorescence ratio \pm SEM using cellular preparations from 6 animals per experimental group. **K-N**, Shown are the expression levels of catalase, TRX, SOD1 and GPX4 normalized to GAPDH. Samples were collected from 6 individual animals per each group. Data expressed as mean \pm SEM. * P <0.05, ** P <0.01, *** P <0.001, and **** P <0.0001 and it is calculated using two-way analysis of variance (ANOVA) with Tukey's post hoc multiple comparison.

Next, we tested the ability of the myocyte antioxidant stress defense system to scavenge and limit oxidative stress caused by exposure of cells to exogenous 100 μ M H_2O_2 . As shown in Figures 6G and 6J, addition of H_2O_2 raised the 405/488 ratios in all groups with expressed roGFP2-ORP1 sensor, confirming that the myocytes sensed the higher oxidative stress. The oxidative stress was higher in db/db versus WT myocytes from mice fed the control diet, but the response to H_2O_2 was significantly reduced by the KE diet in db/db myocytes, in both mitochondrial compartment and cytosolic compartments (Figures 6G and 6H). With redox roGFP2-GRX1 sensors, addition of exogenous H_2O_2 to cardiomyocytes from WT mice fed either the control or KE diet shifted the GSSG/GSH ratio toward the oxidative state, which was observed in diabetic cardiomyocytes at the basal state (Figures 6I and 6J). Addition of H_2O_2 to diabetic cardiomyocytes did not change the GSSG/GSH ratio significantly more compared with the basal state. The KE diet had a small effect on GSSG/GSH ratio in the diabetic group after H_2O_2 addition, preserving GSH level from further oxidation. Altogether, these data indicate that mild elevation in β -OHB via KE diet suppressed the basal level of the oxidative stress in T2D animals, preserved GSH pools and increased their antioxidant capacity.

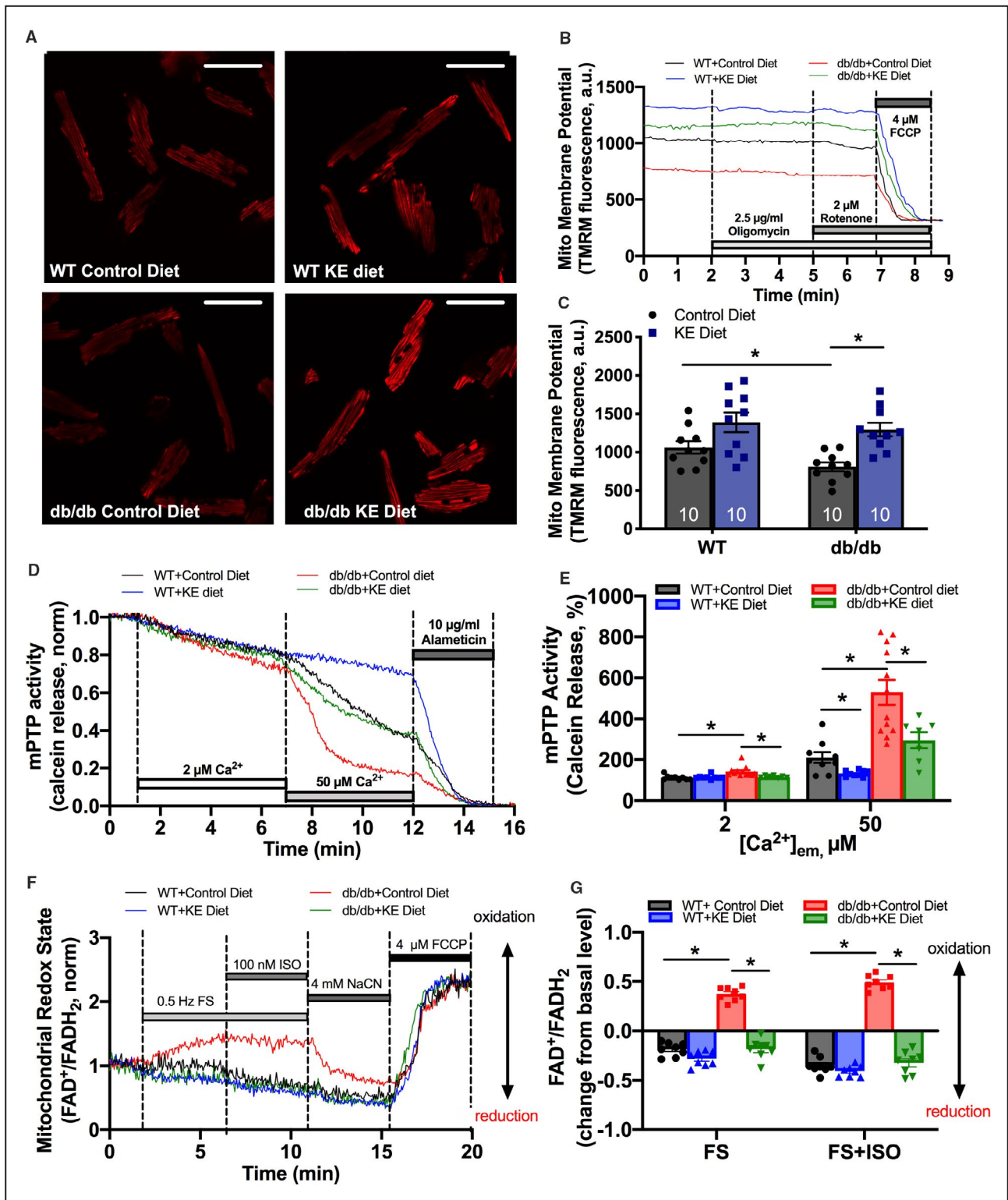
To gain some mechanistic insight of the increased resistance to the oxidative and redox stress, we examined the expression of several enzymes involved in the antioxidative stress defense. We found that catalase (catalyzes the decomposition of H_2O_2 to water and oxygen) expression was elevated in both WT (+37%; n =6 hearts; P =0.052) and diabetic mice (+79%; n =6 hearts; P <0.001) fed a KE diet compared with the corresponding groups on control diets (Figure 6K). At the same time, thioredoxin expression in the heart was significantly decreased in diabetic mice on the control diet (-28%; n =6; P <0.05) compared with WT animals on the control diet (Figure 6L), which was restored back to WT level in the hearts from db/db mice fed the KE

diet (101.7 \pm 3.66% of WT on the control diet; n =6; P =0.4). No changes were found in SOD1, converts superoxide to H_2O_2 and dioxygen) expression between the 4 experimental groups (Figure 6M), while GPX4 catalyzes the reduction of organic hydroperoxides and hydrogen peroxide by glutathione, Figure 6N) was increased only in diabetic mice fed the KE diet by 51% (n =6; P <0.001). Raw bands are shown in Figure S4. These data indicate that the KE diet confers protection against oxidative stress due to upregulation of catalase and thioredoxin. Increase in glutathione peroxidase expression in the diabetic heart on the KE diet could play a role in preservation of the glutathione pool.

Ketone ester (KE) Diet Increases Mitochondrial Membrane Potential, Maintains Redox Potential, and Protects Against mPTP Opening in Diabetic Heart

Using the membrane-potential sensitive dye tetramethylrhodamine methyl ester, we detected that mitochondrial membrane potential ($\Delta\Psi_m$) was significantly decreased in cardiomyocytes from db/db mice on the control diet (Figures 7A through 7C) compared with the WT mice on the control diet (P <0.05). However, in cardiomyocytes isolated from db/db mice on the KE diet, $\Delta\Psi_m$ was maintained at levels close to those observed in cardiomyocytes from WT mice fed either the control or KE diet (Figure 7C).

Furthermore, Figures 7D and 7E show increased activity of mPTP in permeabilized cardiomyocytes isolated from db/db versus WT mice on the control diet, as indicated by faster loss of mitochondrial calcein upon raising extramitochondrial Ca^{2+} to 50 μ M. However, the mPTP opening was significantly decreased in both WT and db/db myocytes isolated from animals that were fed the KE diet (Figure 7D and 7E). In agreement with these data, we found that FAD/FADH₂ autofluorescence in cardiac myocytes from both WT and db/db animals on the KE diet remained reduced during exposure to 0.5-Hz electrical field



stimulation and subsequent application of 100 nM isoproterenol (Figure 7F and 7G), while FAD/FADH₂ shifted significantly toward an oxidative state in db/db cardiomyocytes on the control diet. These data are in agreement with the data obtained with the redox-sensitive proteins (Figure 6) and indicate that

KE helps to maintain the redox state more reduced in db/db myocytes.

Prevention of mPTP opening and maintenance of $\Delta\Psi_m$ are critical for normal mitochondrial function in the heart. The fact that a moderate elevation in β -OHB (ketosis) protected mitochondria against oxidative stress leading to improved

Figure 7. Ketone ester (KE) diet increases mitochondrial membrane potential, maintains redox potential and protects against mPTP opening in diabetic heart.

A, Mitochondrial membrane potential was monitored in cardiomyocytes with membrane potential sensitive dye tetramethylrhodamine methyl ester (TMRM) as shown in the representative images. Scale bar, 50 μm . **B**, Representative traces of TMRM fluorescence for all four groups are shown. **C**, Summary data of mitochondrial membrane potential after addition of 4 μM carbonyl cyanide 4-(trifluoromethoxy)-phenylhydrazone (FCCP), at the end of each experiment are displayed. **D**, The mitochondrial permeability transition pore (mPTP) activity was assessed using calcein assay. Shown are normalized traces of calcein fluorescence at two different extramitochondrial Ca^{2+} ($[\text{Ca}^{2+}]_{\text{em}}$): 2 and 50 μM in control and diabetic cardiomyocytes on either control or KE diet. **E**, Summary data of mPTP activity all four groups after two different $[\text{Ca}^{2+}]_{\text{em}}$ are shown. **F**, Representative traces of changes in the oxidized to reduced flavin adenine dinucleotide (FAD/FADH₂) autofluorescence recorded in intact wild-type (WT) and db/db cardiac myocytes upon electrical field stimulation at 0.5 Hz and subsequent stimulation with 100 nM isoproterenol (ISO). **G**, Summary data of the redox potential changes in cardiomyocytes from WT and db/db animals fed control or KE diet. $n=10\text{--}32$ cells, isolated from 3 mice per group. Data expressed as mean \pm SEM. * $P<0.05$, ** $P<0.01$, *** $P<0.001$, and **** $P<0.0001$ and it is calculated using two-way analysis of variance (ANOVA) with Tukey's post hoc multiple comparison.

$\Delta\Psi_{\text{m}}$ and redox balance maintenance suggests that KE supplementation may be beneficial for patients with T2DM.

KE Diet Enhanced Mitochondrial Quality Control in Diabetic Mice

We have previously reported^{27,54} that β -OHB enhanced mitochondrial repair and elimination of damaged mitochondria in the aged hearts, but not in hearts with advanced HF. We, therefore, examined whether mitochondrial quality control was compromised in diabetic mitochondria and whether a mild elevation in β -OHB via a KE diet could improve mitophagic flux. It is known that damaged mitochondria can be eliminated by selective mitophagy, initiated by the mitochondrial kinase PINK1 and the cytosolic ubiquitin ligase Parkin with subsequent LC3-mediated autophagosome formation and degradation of dysfunctional mitochondria by lysosomes.^{54,55} We, therefore, monitored Parkin accumulation in mitochondria via expression of mCherry-Parkin adenoviral construct, which produced a puncta-like increase in mCherry fluorescence upon Parkin translocation to the mitochondria. Autophagosome formation was monitored by expression of GFP-LC3 adenoviral construct simultaneously with mCherry-Parkin as previously described.^{27,52} Representative images of myocytes expressing these constructs are shown in Figures 8A and 8B for each experimental group. We determined that cell size in db/db myocytes on control diet was slightly smaller compared with the WT group (Figure 8C). We, therefore, normalized Parkin and LC3 count for each experimental condition to the cell size and reported as puncta count per μm^2 .

As shown in Figure 8A (left panel images), WT myocytes isolated from mice fed a control diet showed minimal Parkin-mediated puncta and LC3-mediated autophagosome accumulation in accordance with low levels of oxidative stress detected in these cells under basal conditions. To verify that we could readily detect Parkin and LC3-puncta accumulation in response to mitochondrial stress, we exposed these cells to 100 nM of mitochondrial uncoupler FCCP for

24 hours. This procedure led to partial depolarization of the mitochondrial membrane potential, and induced accumulation of both Parkin and LC3 puncta (red bars) in WT cells (Figure 8C). In separate experiments, cardiomyocytes were exposed to 100 nM bafilomycin A, a vacuolar H⁺-ATPase inhibitor that prevents autophagosome and lysosome fusion (blue bars), and then treated with 100 nM FCCP (green bars) to stimulate mitophagy. As shown in Figure 8C, mCherry-Parkin count was not affected by bafilomycin A1 compared with FCCP alone; however, there was a significant increase in LC3-mediated autophagosome count (green bars), suggesting that mitophagic flux and subsequent autophagosome degradation by lysosome was arrested by bafilomycin A1, thereby leading to the maximal accumulation of the LC3 puncta.

Surprisingly, despite the significant increase in basal oxidative stress (Figure 6) and loss of membrane potential (Figure 7) in the db/db group on the control diet, we saw no increase in Parkin accumulation in db/db myocytes and only a moderate increase in LC3-mediated autophagosome formation (Figures 8D and 8E). This suggests an impaired recruitment of the mitochondrial quality control process in db/db mouse myocytes. In contrast, cardiomyocytes from db/db mice on the KE diet exhibited increased Parkin and LC3-mediated puncta formation (Figure 8D and 8E). This is consistent with the KE diet causing restoration of appropriately enhanced mitophagic flux in db/db mice, even though oxidative and mPTP stress was also limited by the KE diet.

Next, we examined the expression of several proteins in the PINK-Parkin mitophagy pathway in cardiac tissues from diabetic and WT hearts: PINK-1, Mfn2, Parkin, SQSTM1/p62, pro-LC3, and LC3B-II (Figure S5). As shown in Figure 8F, the expression of the serine-threonine protein kinase PINK1 was significantly increased in diabetic mice on the control diet compared with WT mice on the control diet (188 \pm 21% of WT+control diet; $n=12$ hearts). KE diet increased PINK1 expression in WT group (165 \pm 17% of WT+control diet; $n=12$ hearts), but did not induce the further increase

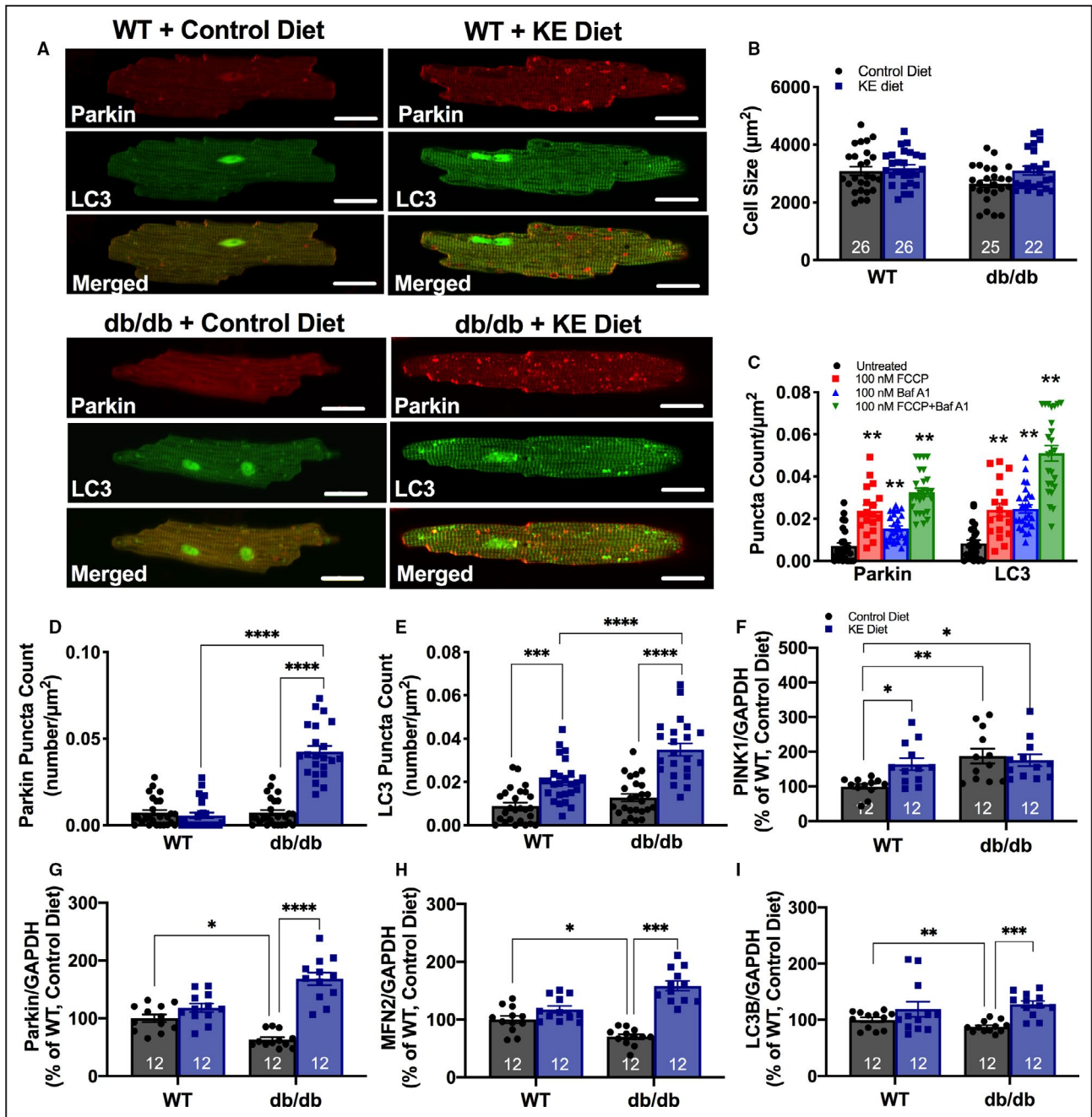


Figure 8. Ketone ester (KE) diet enhanced mitochondrial quality control in diabetic mice.

A, Representative images of mCherry-linked E3 ubiquitin ligase Parkin (mCherry-Parkin) and green fluorescent protein-linked microtubule-associated protein light chain 3 (GFP-LC3) puncta accumulation in untreated myocytes from wild-type (WT) mice fed either control (left) or KE (right) diet are shown. Scale bar, 25 μm . **B**, Cardiac myocytes from diabetic hearts were smaller compared with WT and db/db myocytes on KE diet. **C**, Summary of mCherry-Parkin and GFP-LC3 puncta count per μm^2 in untreated WT cardiomyocytes and myocytes treated with 100 nM carbonyl cyanide 4-(trifluoromethoxy)-phenylhydrazone (FCCP), 100 nM bafilomycin A, or treated with 100 nM bafilomycin A and FCCP, simultaneously. All scale bars correspond to 25 μm . **D**, Summary bars reflect Parkin puncta accumulation in WT and db/db myocytes either on control or KE diet. **E**, Summary bars represent LC3-mediated autophagosome formation count in WT and db/db myocytes either on control or KE diet. $n=18-26$ cells, isolated from 3 mice per group. **F**, PTEN-induced putative kinase 1 (PINK1) expression normalized to GAPDH in WT and db/db hearts in control and KE diet. **G**, Parkin expression normalized to GAPDH in WT and db/db hearts in control and KE diet. **H**, Mitofusin 2 (Mfn2) expression normalized to GAPDH in WT and db/db hearts in control and KE diet. **I**, LC3B-II expression normalized to GAPDH in WT and db/db hearts in control and KE diet. Data expressed as mean \pm SEM. * $P<0.05$, ** $P<0.01$, *** $P<0.001$, and **** $P<0.0001$ and it is calculated using 2-way ANOVA with Tukey's post hoc multiple comparison.

in PINK1 expression in the db/db group ($176 \pm 17\%$ of WT+control diet; $n=12$ hearts). Typically, a decrease in the mitochondrial inner membrane potential stabilizes PINK1 on damaged mitochondria, marking them for Parkin binding, ubiquitination, and mitophagic elimination.⁵⁶ We then examined Parkin, the E3 ubiquitin ligase, expression and determined that Parkin expression was significantly decreased in diabetic hearts on the control diet ($63 \pm 4\%$ of WT on control diet; $n=12$ hearts; $P < 0.001$) (Figure 8G). The KE diet significantly increased Parkin expression in db/db hearts (266% of db/db hearts on control diet; $n=12$; $P < 0.001$), corroborating the data observed in Figure 8D with Parkin puncta count. We have previously demonstrated⁵⁷ that expression of the mitochondrial outer membrane GTPase Mfn2, which mediates Parkin recruitment to damaged mitochondria and creates a hub for autophagosome formation,⁵⁸ was significantly decreased in the failing rabbit heart. We therefore evaluated whether decrease in Parkin accumulation in mitochondria was mediated by impaired Mfn2 expression and inability of mitochondria to recruit Parkin. Indeed, as shown in Figure 8H, Mfn2 expression was decreased in db/db control diet hearts ($70 \pm 4.26\%$ of WT control diet; $n=12$), and increased even above WT levels in diabetic hearts on the KE diet ($158 \pm 8.46\%$ of WT+control diet; $n=12$).

The decrease in Parkin expression also corresponded with decreased LC3B-II ($88 \pm 3\%$ of WT on control diet; $n=12$ hearts; $P < 0.05$) expression in db/db control diet hearts, which reflects the amount of LC3B-II fused with autophagosome (Figure 8I). The KE diet significantly increased LC3B-II expression ($146 \pm 6\%$ of db/db+control diet; $n=12$; $P < 0.005$). LC3B is a mammalian autophagosomal marker (an analog of Atg8 in yeasts) which is translated as a full-length 30 kDa pro-LC3 precursor.⁵⁹ Then, pro-LC3 is cleaved at the C-terminus to form the cytosolic LC3B-I (18 kDa). Sequentially, LC3B-I is converted to LC3B-II (16 kDa) that gets recruited to autophagosomal membranes via conjugation to phosphatidylethanolamine.⁶⁰ The conversion of cytosolic LC3-I to its lipidated membrane-bound form LC3-II indicates autophagosome formation, and the amount of LC3-II typically correlates with the number of autophagosomes.^{59,60} The autophagic adaptor protein SQSTM1/p62 (62 kDa) which is recruited to the clustered mitochondria and links ubiquitinated mitochondrial protein aggregates with LC3B-II, facilitates the degradation of autophagosome formation. As shown in Figure S5, the expression level of pro-LC3 was also decreased in diabetic hearts on the control diet ($66 \pm 4\%$ of WT on control diet; $n=12$ hearts; $P < 0.05$) and increased in db/db hearts on the KE diet ($141 \pm 7\%$ of WT+control diet; $n=12$). The expression levels of the adaptor protein SQSTM1/p62 (62 kDa) (Figure S5G) did not change significantly in the diabetic heart (even though it was slightly elevated $124 \pm 7\%$ compared with

WT); however, it was increased by the KE diet in both WT ($143 \pm 6\%$ of WT+control diet; $n=12$) and db/db ($147 \pm 7\%$ of WT+control diet, $n=12$) hearts.

Taken together, these data indicate that diabetic hearts on control diet exhibited an impaired ability to remove damaged mitochondria via mitophagy compared with the WT hearts. The impairment seemed to be associated with decreased expression of Mfn2, which resulted in decreased Parkin recruitment to the mitochondria and LC3-mediated autophagosome formation. The elevation in β -OHB levels via KE diet enhanced mitophagic flux, which would be expected to promote mitochondrial repair and removal of damaged mitochondria in the diabetic heart.

DISCUSSION

In this study, we examined whether moderate dietary ketosis induced by KE supplementation improved cardiac function in db/db mice, a model of T2D. The levels of circulating β -OHB achieved via KE supplementation in our study were within therapeutic range of ketones (3.0–6.0 mM) recommended for medical conditions such as epilepsy, cancer, and metabolic disorders.^{35,61} KE supplementation had salutary effects on both systolic and diastolic function, mitochondrial oxidative stress, membrane potential, redox balance, mPTP activity, and mitophagy. T2DM (non-insulin-dependent), the most prevalent form (90%–95%) of diabetes mellitus, is becoming a global epidemic among children and adults.⁶² Patients with diabetes mellitus have an almost 2-fold higher risk of developing HF than patients without diabetes mellitus.^{62–64} However, despite the success of many commonly used antihyperglycemic therapies to lower high blood glucose levels in patients with T2DM, the high occurrence of HF persists.⁶² This suggests that additional factors beyond hyperglycemia contribute to the increased HF risk in T2DM, and therefore new alternative therapies are urgently needed to prevent HF development in patients with T2DM. Furthermore, recent studies^{65,66} have demonstrated that sodium-glucose cotransporter 2 inhibitors decrease the risk of HF in patients with T2DM. While the mechanism of action of these inhibitors is not completely understood, several studies observed a corresponding moderate elevation in circulating levels of β -OHB and acetoacetate that correlated with the improvement of LV function.^{65–68}

As a model of T2DM, we used a well-established db/db mouse model that has a pathogenesis of T2DM development similar to humans⁶⁹ with initial insulin resistance followed by an insulin secretion defect.^{70,71} The KE diet led to a significant elevation of circulating β -OHB concentration in both db/db and WT mice (Figure 1D), with a corresponding decrease in circulating glucose levels in diabetic mice (Figure 1E). This

indicates that a shift in metabolism toward ketone usage led to a beneficial decrease in plasma glucose levels. Indeed, a recent study⁷² reported that KE ingestion before the oral glucose test attenuates the glyce-mic response in healthy young individuals. Animals on the KE diet (both WT and db/db) gained slightly more weight (even through it was not significant) compared with the animals on the control diet (Figure 1F) despite a similar caloric uptake. These data are consistent with prior studies^{73,74} where mice fed either a high-fat or ke-togenic diet ad libitum gained more weight compared with the control groups. It was shown⁷³ that calorie re-striction or a cyclic ketogenic diet (similar to intermittent fasting) were required to control weight gain and imitate the benefits of intermittent fasting eventually leading to the reduced midlife mortality in aging C57BL/6 mice.

Improvement in Systolic and Diastolic Functions in db/db Mice on the KE Diet

As shown in Figure 2, diabetic mice fed the control diet had evidence of systolic and diastolic dysfunction, while the KE diet improved both systolic and diastolic function. Specifically, the KE diet preserved both cardiac dimensions and fractional shortening, suggesting that a moderate increase in β -OHB can prevent cardiac dysfunction when applied at the early stages of disease. A decrease in cardiac dimensions concurrent with a decline in cardiac function in db/db mice was surprising to us; however, these data are in agreement with another study⁷⁵ that also demonstrated that db/db mice in fact have smaller hearts. Furthermore, another study showed that db/db mice do not develop cardiac hypertrophy and HF following transverse aortic constriction,⁷⁶ but nearly half of db/db mice subjected to transverse aortic constriction died soon after the surgery, suggestive of lower metabolic flexibility.

Suppression of Oxidative Stress and mPTP Opening in Diabetic Hearts by KE Diet

Our study also found that KE efficiently suppressed elevated oxidative stress in diabetic hearts (Figure 6), prevented mPTP opening and shift of redox potential toward oxidation (Figures 6 and 7), and enhanced mitochondrial quality control via mitophagy (Figure 8). We found that despite a decrease in mitochondrial membrane potential (Figure 7) and increase in oxidative stress (Figure 6), the level of Parkin puncta accumulation and LC3-mediated autophagosome formation in diabetic mitochondria was extremely low (Figure 8), indicating impaired mitophagy. Indeed, several studies^{77–79} suggested that the proper removal and recycling of damaged mitochondria via mitochondrial quality control in the heart are essential for protecting

cardiac myocytes against adverse effects of diabetic cardiomyopathy. A study performed in peripheral blood mononuclear cells collected from human patients with prediabetes and T2D revealed that autophagy was upregulated in samples from patients with pre-diabetes, but severely impaired in advanced T2DM.⁸⁰ We also recently demonstrated that PINK-1/Parkin-mediated mitophagy was impaired in advanced rabbit HF model.²⁷ We found that in HF myocytes, increased numbers of mitochondria were marked with Parkin for degradation; however, LC3-mediated autophagosome formation was impaired, which led to Parkin buildup at elevated levels. Interestingly, cardiac myocytes treated with 2 mM β -OHB improved PINK-1/Parkin-mediated mitophagy in aged cardiomyocytes, but not in HF myocytes. We further demonstrated that the impairment of mitochondrial quality control was related to diminished function of Mfn2 in HF. Cardiomyocytes treated with cell-permeable TAT-MP1^{Gly} peptide, which stabilized Mfn2 conformation, significantly improved mitophagy in HF myocytes.

Our current study also identified a significant decrease in Mfn2 expression in diabetic mice on control diet (Figure 8 and Figure S5). Placing mice on the KE diet prevented the decline in Mfn2 expression and improved Parkin translocation to the mitochondria. We believe that β -OHB affects Parkin translocation via modulation of oxidative stress and Mfn2 expression. Several studies^{81,82} reported that a decrease in Mfn2 expression inversely correlated with oxidative and redox stress. It was shown that Mfn2 overexpression restored Parkin translocation in Angiotensin-induced model of heart failure. Furthermore, Mfn2 deficiency and oxidative stress contributed to insulin resistance in rat skeletal muscle cells.⁸² These facts, together with our current data in Figure 8, indicate that ketones can limit cardiac dysfunction by improving mitophagy and mitochondrial repair in the absence of severe structure remodeling as observed in advanced HF.

Mechanistic Roles of SCOT and ACAT1 Enzymes in the Diabetic Heart Treated with KE Diet

We found that the KE diet restored diminished expression of BDH1 in the diabetic heart back to normal but more importantly, almost doubled expression of SCOT and increased ACAT1 expression by 25% (Figure 3). Horton et al²¹ demonstrated that cardiospecific knock-out of BDH1 led to inability of the heart to utilize ketone bodies and was associated with worsening of heart failure in response to transverse aortic constriction-induced pressure overload combined with an ischemic insult when compared with WT controls subjected to similar procedures. Similarly, transgenic mice with overexpressed BDH1 had less pathologic

remodeling in response to transverse aortic constriction.⁸³ Furthermore, other studies have reported that aging⁸⁴ and oxidative stress observed in HF⁸⁵ decrease expression and activity of SCOT by nearly 50%. When ketone bodies are delivered to the heart, β -OHB is oxidized back to acetoacetate by the mitochondrial D- β -hydroxybutyrate dehydrogenase (Figure 3A). The metabolism of ketone bodies in the heart requires a unique enzyme that is not present in the ketone body biosynthetic pathway in the liver, SCOT, which converts acetoacetate to acetoacetyl-CoA. SCOT uses succinyl-CoA in the TCA cycle as the CoA donor, forming succinate and acetoacetyl-CoA. Next, mitochondrial ACAT1 cleaves the acetoacetyl-CoA into 2 molecules of acetyl-CoA, which can generate energy by entering the TCA cycle pathway (Figure 3).

SCOT activity is tightly coupled to the activity of mitochondrial complex II in the heart. The fact that KE supplementation upregulated SCOT expression to a higher degree in both WT and T2DM mice suggest that the activity of complex II would be also increased by KE. This, in fact, is evident by the increase in basal mitochondrial respiration when mitochondria were respiring on Complex II substrate succinate (Figure 4A and 4B) in KE groups. Thus, in addition to providing the acetyl-CoA to the TCA cycle, the increase in SCOT expression can also increase complex II activity.

The role of β -OHB in T2DM and HF is not completely understood; however, growing evidence indicates that ketones can serve as an emergency fuel under HF conditions when the use of the main fuel for the heart, fatty acids, is compromised.^{19–21} The recent study from the Lopaschuk group¹⁸ confirmed the role of ketones as the essential fuel source in the failing heart; however, an increase in ketone body metabolism did not lead to an improvement of cardiac work and efficiency in the failing heart. Horton et al²¹ demonstrated that the failing heart uses β -OHB as a metabolic stress defense and was able to compensate for the decrease in fatty acid oxidation. Our data demonstrate that KE was able to increase both basal (Figure 4E) and ADP-induced respiration (Figure 4F) in isolated cardiac mitochondria, but it did not lead to the increase in respiratory control ratio (Figure 4G). This could be attributable to the fact that mitochondria in db/db hearts were already partially uncoupled, which is evident by the increase in oxidative stress (Figure 6), decrease in mitochondrial membrane potential (Figures 7A through 7C) and increase in mPTP activity (Figures 7D and 7E). The uncoupling effect could mask the potential increase in oxidative phosphorylation eventually leading to zero net change in mitochondrial coupling.

Here, we demonstrated that a KE diet decreased oxidative and redox stress, decreased mPTP opening and enhanced mitochondrial quality control in type 2 diabetic hearts, resulting in improved cardiac function.

An increased incidence for cell death in diabetic human hearts was related to an increased sensitivity of mPTP opening.⁸⁶ Therefore, the preservation of mitochondrial function could also involve energy-independent effects of ketone bodies as we described here. We found that several enzymes involved in antioxidant stress defense were upregulated by the KE diet. Specifically, we observed an \approx 80% increase in catalase and \approx 50% increase in GPX4 expression in diabetic hearts on a KE diet. Notably, there was no decrease in expression of these enzymes in diabetic hearts on a control diet. SOD1 expression in diabetic hearts was similar to the WT group and was not affected by a KE diet. However, the expression of thioredoxin was decreased in diabetic hearts on a control diet by 28% compared with WT animals on a control diet (Figure 6L). This decline in thioredoxin expression in the diabetic heart was more than completely recovered by KE diet. While both catalase and GPX4 catalyze the reduction of H_2O_2 to water and oxygen, the glutathione peroxidases are reported to be more efficient in H_2O_2 decomposition and also catalyze the reduction of peroxide radicals to alcohols and oxygen using GSH as an electron donor.⁸⁷ Specifically, GPX4 is present in relatively high amounts in cardiac tissue, in both cytosolic and mitochondrial compartments.⁸⁸

Prior studies performed in skeletal muscles of both rodents and humans⁸⁹ demonstrated a direct correlation between high-fat diet ingestion, increased H_2O_2 generation, and a decrease in the redox-balancing capacity of the muscle in the absence of any change in mitochondrial respiratory function. Similarly, glucose ingestion induced almost 2-fold increase in GSSG levels, and \approx 50% increase in GSSG/GSH ratio toward oxidation. Interestingly, overexpression of catalase in muscle mitochondria completely preserved insulin sensitivity despite a high-fat diet. Furthermore, it was demonstrated that overexpression of glutathione peroxidase attenuated diabetes mellitus–induced cardiac dysfunction.⁹⁰ Glutathione peroxidases are reported to exhibit greater protective effects against oxidative stress compared with SOD1 and catalases. Therefore, it is plausible to conclude that KE can protect the heart via chronic elevation in the expression of several enzymes that are involved in ketone body metabolism and protection against oxidative and redox stress.

Limitations

Our study was performed in a murine animal model of T2DM, and therefore the results of our study may not be directly extrapolated to human T2DM. However, the db/db mouse is a well-accepted T2DM model that recapitulates most aspects of the human disease. Since the db/db model has the feature of overt insulin resistance, progressive development of hyperglycemia and

β -cell dysfunction with age, it has the merit of having close clinical relevance to human T2DM.

To keep the calorie uptake similar between KE and control groups, the carbohydrate content of the KE diet was reduced as shown in Table. Clinical studies show that a decrease in the carbohydrate content of the patient's diet can lead to a mild ketosis by itself, and a decline in circulating glucose and insulin levels in patients with T2DM.^{91,92} However, nearly a double increase in circulating β -OHB concentration was reported in these studies, and therefore it is not clear whether a decrease in carbohydrate content or an increase in β -OHB levels was responsible for the beneficial effects observed in these clinical studies.

CONCLUSIONS

In summary, this is the first study to document that KE supplementation can prevent the development of cardiac dysfunction and progression toward HF in T2DM. A KE diet resulted in a significant elevation in circulating β -OHB levels, which prevented the development of cardiac dysfunction in diabetic mice. In contrast to the nondiabetic failing hearts, fatty acid metabolism was increased in the diabetic heart. This would preclude the use of the "traditional" ketogenic diet, which requires a significant increase in fat intake and complete elimination of carbohydrates from the diet to maintain ketosis, which can facilitate the development of fatty acid toxicity observed in patients with T2DM.

ARTICLE INFORMATION

Received May 4, 2021; accepted July 19, 2021.

Affiliations

Department of Internal Medicine, Cardiovascular Medicine (P.N.T., S.S., N.C.), Department of Pharmacology (C.V.M., D.M.B., E.N.D.) and Department of Molecular Biosciences (E.N.D.), University of California, Davis, CA; Laboratory of Metabolic Control, National Institute on Alcohol Abuse and Alcoholism, National Institutes of Health, Rockville, MD (M.T.K., R.L.V.); and Department of Veterans Affairs, Northern California Health Care System, Mather, CA (S.S., N.C.).

Acknowledgments

We also thank Michael Nguyen, Johanna M. Borst, Landon Sims, Tjien Dwyer and Logan R. Bailey for the expert technical assistance. Author Contributions: All authors contributed significantly to this work. Dr Dedkova was the principal investigator for this study: She designed, sponsored and supervised this project. Dr Thai, C.V. Miller, and Dr Dedkova performed experiments and analyzed the data. Dr Dedkova and Dr Thai wrote the manuscript. M.T. King and Dr Veech synthesized KE and contributed to the editing of the manuscript. Dr Chiamvimonvat provided expertise and edited the manuscript. Drs Schaefer and Bers edited the manuscript and provided financial support.

Sources of Funding

This project was supported by the National Institute of Health 1R01HL155907-1 (to Dr Dedkova), American Heart Association Grant-In-Aid 15GRNT25090220 (to Dr Dedkova), Friedreich's Ataxia Research Alliance

award (to Dr Dedkova), University of California Davis CRCF Pilot & Feasibility Award 181031 (to Dr Dedkova), and the University of California Innovative Development Award (to Dr Dedkova), postdoctoral fellowship from NIH T32 HL086350 Training Grant in Basic & Translational Cardiovascular Science and NIH F32 HL149288 (to Dr Thai), NIH R01 HL132831 (to Dr Bers), NIH R01 HL085727 (to Dr Chiamvimonvat) and NIH S10 RR033106 (in vivo ultrasound imaging system).

Disclosures

None.

Supplementary Material

Data S1
Table S1
Figures S1–S5

REFERENCES

- Benjamin EJ, Blaha MJ, Chiuve SE, Cushman M, Das SR, Deo R, de Ferranti SD, Floyd J, Fornage M, Gillespie C, et al. Heart disease and stroke statistics-2017 update: a report from the American Heart Association. *Circulation*. 2017;135:e146–e603.
- Fillmore N, Mori J, Lopaschuk GD. Mitochondrial fatty acid oxidation alterations in heart failure, ischaemic heart disease and diabetic cardiomyopathy. *Br J Pharmacol*. 2014;171:2080–2090. DOI: 10.1111/bph.12475.
- Seferovic PM, Paulus WJ. Clinical diabetic cardiomyopathy: a two-faced disease with restrictive and dilated phenotypes. *Eur Heart J*. 2015;36(1718–1727):1727a–1727c.
- Paolillo S, Marsico F, Prastaro M, Renga F, Esposito L, De Martino F, Di Napoli P, Esposito I, Ambrosio A, Iannuberto M, et al. Diabetic cardiomyopathy: definition, diagnosis, and therapeutic implications. *Heart Fail Clin*. 2019;15:341–347. DOI: 10.1016/j.hfc.2019.02.003.
- Fillmore N, Lopaschuk GD. Targeting mitochondrial oxidative metabolism as an approach to treat heart failure. *Biochim Biophys Acta*. 2013;1833:857–865. DOI: 10.1016/j.bbamcr.2012.08.014.
- Isfort M, Stevens SC, Schaffer S, Jong CJ, Wold LE. Metabolic dysfunction in diabetic cardiomyopathy. *Heart Fail Rev*. 2014;19:35–48. DOI: 10.1007/s10741-013-9377-8.
- Forcheron F, Basset A, Abdallah P, Del Carmine P, Gadot N, Beylot M. Diabetic cardiomyopathy: effects of fenofibrate and metformin in an experimental model—the Zucker diabetic rat. *Cardiovasc Diabetol*. 2009;8:16. DOI: 10.1186/1475-2840-8-16.
- Nissen SE, Wolski K. Effect of rosiglitazone on the risk of myocardial infarction and death from cardiovascular causes. *N Engl J Med*. 2007;356:2457–2471. DOI: 10.1056/NEJMoa072761.
- Karwi QG, Uddin GM, Ho KL, Lopaschuk GD. Loss of metabolic flexibility in the failing heart. *Front Cardiovasc Med*. 2018;5:68. DOI: 10.3389/fcvm.2018.00068.
- Lopaschuk GD, Ussher JR, Folmes CD, Jaswal JS, Stanley WC. Myocardial fatty acid metabolism in health and disease. *Physiol Rev*. 2010;90:207–258. DOI: 10.1152/physrev.00015.2009.
- Neubauer S. The failing heart—an engine out of fuel. *N Engl J Med*. 2007;356:1140–1151. DOI: 10.1056/NEJMra063052.
- Neubauer S, Horn M, Cramer M, Harre K, Newell JB, Peters W, Pabst T, Ertl G, Hahn D, Ingwall JS, et al. Myocardial phosphocreatine-to-ATP ratio is a predictor of mortality in patients with dilated cardiomyopathy. *Circulation*. 1997;96:2190–2196. DOI: 10.1161/01.CIR.96.7.2190.
- Aubert G, Vega RB, Kelly DP. Perturbations in the gene regulatory pathways controlling mitochondrial energy production in the failing heart. *Biochim Biophys Acta*. 2013;1833:840–847. DOI: 10.1016/j.bbamcr.2012.08.015.
- Thai PN, Daugherty DJ, Frederich BJ, Lu X, Deng W, Bers DM, Dedkova EN, Schaefer S. Cardiac-specific conditional knockout of the 18-kDa mitochondrial translocator protein protects from pressure overload induced heart failure. *Sci Rep*. 2018;8:16213. DOI: 10.1038/s41598-018-34451-2.
- Abel ED. Obesity stresses cardiac mitochondria even when you are young. *J Am Coll Cardiol*. 2011;57:586–589. DOI: 10.1016/j.jacc.2010.09.039.
- Boudina S, Bugger H, Sena S, O'Neill BT, Zaha VG, Ilkun O, Wright JJ, Mazumder PK, Palfreyman E, Tidwell TJ, et al. Contribution of impaired

- myocardial insulin signaling to mitochondrial dysfunction and oxidative stress in the heart. *Circulation*. 2009;119:1272–1283. DOI: 10.1161/CIRCULATIONAHA.108.792101.
17. Chong CR, Clarke K, Levelt E. Metabolic remodeling in diabetic cardiomyopathy. *Cardiovasc Res*. 2017;113:422–430.
 18. Ho KL, Zhang L, Wagg C, Al Batran R, Gopal K, Levesseur J, Leone T, Dyck JRB, Ussher JR, Muoio DM, et al. Increased ketone body oxidation provides additional energy for the failing heart without improving cardiac efficiency. *Cardiovasc Res*. 2019;115:1606–1616. DOI: 10.1093/cvr/cvz045.
 19. Aubert G, Martin OJ, Horton JL, Lai L, Vega RB, Leone TC, Koves T, Gardell SJ, Krüger M, Hoppel CL, et al. The failing heart relies on ketone bodies as a fuel. *Circulation*. 2016;133:698–705. DOI: 10.1161/CIRCULATIONAHA.115.017355.
 20. Bedi KC, Snyder NW, Brandimarto J, Aziz M, Mesaros C, Worth AJ, Wang LL, Javaheri A, Blair IA, Margulies KB, et al. Evidence for intramyocardial disruption of lipid metabolism and increased myocardial ketone utilization in advanced human heart failure. *Circulation*. 2016;133:706–716. DOI: 10.1161/CIRCULATIONAHA.115.017545.
 21. Horton JL, Davidson MT, Kurishima C, Vega RB, Powers JC, Matsuura TR, Petucci C, Lewandowski ED, Crawford PA, Muoio DM, et al. The failing heart utilizes 3-hydroxybutyrate as a metabolic stress defense. *JCI Insight*. 2019;4:e124079. DOI: 10.1172/jci.insight.124079.
 22. Dedkova EN, Blatter LA. Role of beta-hydroxybutyrate, its polymer poly-beta-hydroxybutyrate and inorganic polyphosphate in mammalian health and disease. *Front Physiol*. 2014;5:260.
 23. Veech RL, Bradshaw PC, Clarke K, Curtis W, Pawlosky R, King MT. Ketone bodies mimic the life span extending properties of caloric restriction. *IUBMB Life*. 2017;69:305–314. DOI: 10.1002/iub.1627.
 24. Cahill GF Jr. Fuel metabolism in starvation. *Annu Rev Nutr*. 2006;26:1–22. DOI: 10.1146/annurev.nutr.26.061505.111258.
 25. Mizuno Y, Harada E, Nakagawa H, Morikawa Y, Shono M, Kugimiya F, Yoshimura M, Yasue H. The diabetic heart utilizes ketone bodies as an energy source. *Metabolism*. 2017;77:65–72. DOI: 10.1016/j.metabol.2017.08.005.
 26. Shimazu T, Hirschey MD, Newman J, He W, Shirakawa K, Le Moan N, Grueter CA, Lim H, Saunders LR, et al. Suppression of oxidative stress by beta-hydroxybutyrate, an endogenous histone deacetylase inhibitor. *Science*. 2013;339:211–214.
 27. Thai PN, Seidlmayer LK, Miller C, Ferrero M, Dorn li GW, Schaefer S, Bers DM, Dedkova EN. Mitochondrial quality control in aging and heart failure: Influence of ketone bodies and mitofusin-stabilizing peptides. *Front Physiol*. 2019;10:382. DOI: 10.3389/fphys.2019.00382.
 28. Kruljac I, Cacic M, Cacic P, Ostojic V, Stefanovic M, Sikic A, Vrkljan M. Diabetic ketosis during hyperglycemic crisis is associated with decreased all-cause mortality in patients with type 2 diabetes mellitus. *Endocrine*. 2017;55:139–143. DOI: 10.1007/s12020-016-1082-7.
 29. Kessler SK, Neal EG, Camfield CS, Kossoff EH. Dietary therapies for epilepsy: future research. *Epilepsy Behav*. 2011;22:17–22. DOI: 10.1016/j.yebeh.2011.02.018.
 30. Kosinski C, Jornayvaz F. Effects of ketogenic diets on cardiovascular risk factors: evidence from animal and human studies. *Nutrients*. 2017;9(5):517. DOI: 10.3390/nu9050517.
 31. Srivastava S, Kashiwaya Y, King MT, Baxa U, Tam J, Niu G, Chen X, Clarke K, Veech RL. Mitochondrial biogenesis and increased uncoupling protein 1 in brown adipose tissue of mice fed a ketone ester diet. *FASEB J*. 2012;26:2351–2362. DOI: 10.1096/fj.11-200410.
 32. Srivastava S, Baxa U, Niu G, Chen X, Veech RL. A ketogenic diet increases brown adipose tissue mitochondrial proteins and UCP1 levels in mice. *IUBMB Life*. 2013;65:58–66. DOI: 10.1002/iub.1102.
 33. Clarke K, Tchabanenko K, Pawlosky R, Carter E, Knight NS, Murray AJ, Cochlin LE, King MT, Wong AW, Roberts A, et al. Oral 28-day and developmental toxicity studies of (r)-3-hydroxybutyl (r)-3-hydroxybutyrate. *Regul Toxicol Pharmacol*. 2012;63:196–208. DOI: 10.1016/j.yrtph.2012.04.001.
 34. Murray AJ, Knight NS, Cole MA, Cochlin LE, Carter E, Tchabanenko K, Pichulik T, Gulston MK, Atherton HJ, Schroeder MA, et al. Novel ketone diet enhances physical and cognitive performance. *FASEB J*. 2016;30:4021–4032. DOI: 10.1096/fj.201600773R.
 35. Clarke K, Tchabanenko K, Pawlosky R, Carter E, Todd King M, Musaveloso K, Ho M, Roberts A, Robertson J, VanTallie TB, et al. Kinetics, safety and tolerability of (R)-3-hydroxybutyl (R)-3-hydroxybutyrate in healthy adult subjects. *Regul Toxicol Pharmacol*. 2012;63:401–408. DOI: 10.1016/j.yrtph.2012.04.008.
 36. Cox P, Kirk T, Ashmore T, Willerton K, Evans R, Smith A, Murray A, Stubbs B, West J, McLure S, et al. Nutritional ketosis alters fuel preference and thereby endurance performance in athletes. *Cell Metab*. 2016;24:256–268. DOI: 10.1016/j.cmet.2016.07.010.
 37. Troy BL, Pombo J, Rackley CE. Measurement of left ventricular wall thickness and mass by echocardiography. *Circulation*. 1972;45:602–611.
 38. Rogers GW, Brand MD, Petrosyan S, Ashok D, Elorza AA, Ferrick DA, Murphy AN. High throughput microplate respiratory measurements using minimal quantities of isolated mitochondria. *PLoS One*. 2011;6:e21746. DOI: 10.1371/journal.pone.0021746.
 39. Seidlmayer LK, Juettner VV, Kettlewell S, Pavlov EV, Blatter LA, Dedkova EN. Distinct mPTP activation mechanisms in ischaemia-reperfusion: contributions of Ca²⁺, ROS, pH, and inorganic polyphosphate. *Cardiovasc Res*. 2015;106:237–248. DOI: 10.1093/cvr/cvv097.
 40. Seidlmayer LK, Kuhn J, Berbner A, Arias-Loza PA, Williams T, Kaspar M, Czolbe M, Kwong JQ, Molkenin JD, Heinze KG, et al. Inositol 1,4,5-trisphosphate-mediated sarcoplasmic reticulum-mitochondrial crosstalk influences adenosine triphosphate production via mitochondrial Ca²⁺ uptake through the mitochondrial ryanodine receptor in cardiac myocytes. *Cardiovasc Res*. 2016;112:491–501.
 41. Seidlmayer LK, Gomez-Garcia MR, Shiba T, Porter GA Jr, Pavlov EV, Bers DM, Dedkova EN. Dual role of inorganic polyphosphate in cardiac myocytes: the importance of polyphosphate chain length for energy metabolism and mPTP activation. *Arch Biochem Biophys*. 2019;662:177–189. DOI: 10.1016/j.abb.2018.12.019.
 42. Seidlmayer LK, Mages C, Berbner A, Eder-Negrin P, Arias-Loza PA, Kaspar M, Song M, Dorn GW, Kohlhaas M, Frantz S, et al. Mitofusin 2 is essential for IP3-mediated SR/mitochondria metabolic feedback in ventricular myocytes. *Front Physiol*. 2019;10:733. DOI: 10.3389/fphys.2019.00733.
 43. Dedkova EN, Blatter LA. Measuring mitochondrial function in intact cardiac myocytes. *J Mol Cell Cardiol*. 2012;52:48–61. DOI: 10.1016/j.yjmcc.2011.08.030.
 44. Dedkova EN, Seidlmayer LK, Blatter LA. Mitochondria-mediated cardioprotection by trimetazidine in rabbit heart failure. *J Mol Cell Cardiol*. 2013;59:41–54. DOI: 10.1016/j.yjmcc.2013.01.016.
 45. Seidlmayer LK, Gomez-Garcia MR, Blatter LA, Pavlov E, Dedkova EN. Inorganic polyphosphate is a potent activator of the mitochondrial permeability transition pore in cardiac myocytes. *J Gen Physiol*. 2012;139:321–331. DOI: 10.1085/jgp.201210788.
 46. Dey S, Sidor A, O'Rourke B. Compartment-specific control of reactive oxygen species scavenging by antioxidant pathway enzymes. *J Biol Chem*. 2016;291:11185–11197. DOI: 10.1074/jbc.M116.726968.
 47. Gutscher M, Sobotta MC, Wabnitz GH, Ballikaya S, Meyer AJ, Samstag Y, Dick TP. Proximity-based protein thiol oxidation by h2o2-scavenging peroxidases. *J Biol Chem*. 2009;284:31532–31540. DOI: 10.1074/jbc.M109.059246.
 48. Dickinson BC, Srikun D, Chang CJ. Mitochondrial-targeted fluorescent probes for reactive oxygen species. *Curr Opin Chem Biol*. 2010;14:50–56. DOI: 10.1016/j.cbpa.2009.10.014.
 49. Meyer AJ, Dick TP. Fluorescent protein-based redox probes. *Antioxid Redox Signal*. 2010;13:621–650. DOI: 10.1089/ars.2009.2948.
 50. Morgan B, Sobotta MC, Dick TP. Stabilizing e(gsh) and h2o2 with rogp2-based redox probes. *Free Radic Biol Med*. 2011;51:1943–1951. DOI: 10.1016/j.freeradbiomed.2011.08.035.
 51. Schwarzlander M, Dick TP, Meyer AJ, Morgan B. Dissecting redox biology using fluorescent protein sensors. *Antioxid Redox Signal*. 2016;24:680–712. DOI: 10.1089/ars.2015.6266.
 52. Kubli DA, Cortez MQ, Moyzis AG, Najor RH, Lee Y, Gustafsson AB. PINK1 is dispensable for mitochondrial recruitment of Parkin and activation of mitophagy in cardiac myocytes. *PLoS One*. 2015;10:e0130707. DOI: 10.1371/journal.pone.0130707.
 53. Aldakkak M, Stowe DF, Cheng Q, Kwok WM, Camara AK. Mitochondrial matrix K⁺ flux independent of large-conductance Ca²⁺-activated K⁺ channel opening. *Am J Physiol Cell Physiol*. 2010;298:C530–C541.
 54. Thai PN, Demirkhanyan L, King MT, Zakharian E, Veech RL, Schaefer S, Bers DM, Dedkova EN. Ketone bodies and their polymers in heart failure and type 2 diabetes: lessons learned from the ketone ester diet. *Biophys J*. 2019;116:2a–3a. DOI: 10.1016/j.bpj.2018.11.037.
 55. Moyzis AG, Sadoshima J, Gustafsson AB. Mending a broken heart: the role of mitophagy in cardioprotection. *Am J Physiol Heart Circ Physiol*. 2015;308:H183–H192. DOI: 10.1152/ajpheart.00708.2014.
 56. Narendra DP, Jin SM, Tanaka A, Suen DF, Gautier CA, Shen J, Cookson MR, Youle RJ. PINK1 is selectively stabilizing on impaired mitochondria

- to activate Parkin. *PLoS Biol.* 2010;8:e1000298. DOI: 10.1371/journal.pbio.1000298.
57. Thai PN, Seidlmayer LK, Miller C, Ferrero M, Dorn GW II, Schaefer S, Bers DM, Dedkova EN. Mitochondrial quality control in aging and heart failure: influence of ketone bodies and mitofusin-stabilizing peptides. *Front Physiol.* 2019;10:382. DOI: 10.3389/fphys.2019.00382.
 58. Chen Y, Dorn GW 2nd. Pink1-phosphorylated mitofusin 2 is a Parkin receptor for culling damaged mitochondria. *Science.* 2013;340:471–475. DOI: 10.1126/science.1231031.
 59. Kabeya Y, Mizushima N, Ueno T, Yamamoto A, Kirisako T, Noda T, Kominami E, Ohsumi Y, Yoshimori T. LC3, a mammalian homologue of yeast Apg8p, is localized in autophagosomal membranes after processing. *EMBO J.* 2000;19:5720–5728. DOI: 10.1093/emboj/19.21.5720.
 60. Kabeya Y, Mizushima N, Yamamoto A, Oshitani-Okamoto S, Ohsumi Y, Yoshimori T. LC3, GABARAP and GATE16 localize to autophagosomal membrane depending on form-II formation. *J Cell Sci.* 2004;117:2805–2812. DOI: 10.1242/jcs.01131.
 61. Newport MT, Vanlathie TB, Kashiwaya Y, King MT, Veech RL. A new way to produce hyperketonemia: use of ketone ester in a case of Alzheimer's disease. *Alzheimers Dement.* 2015;11:99–103. DOI: 10.1016/j.jalz.2014.01.006.
 62. Kenny HC, Abel ED. Heart failure in type 2 diabetes mellitus. *Circ Res.* 2019;124:121–141. DOI: 10.1161/CIRCRESAHA.118.311371.
 63. Nichols GA, Hillier TA, Erbrey JR, Brown JB. Congestive heart failure in type 2 diabetes: prevalence, incidence, and risk factors. *Diabetes Care.* 2001;24:1614–1619. DOI: 10.2337/diacare.24.9.1614.
 64. Dei Cas A, Khan SS, Butler J, Mentz RJ, Bonow RO, Avogaro A, Tschoepe D, Doehner W, Greene SJ, Senni M, et al. Impact of diabetes on epidemiology, treatment, and outcomes of patients with heart failure. *JACC Heart Fail.* 2015;3:136–145.
 65. Santos-Gallego CG, Requena-Ibanez JA, San Antonio R, Ishikawa K, Watanabe S, Picatoste B, Flores E, Garcia-Ropero A, Sanz J, Hajjar RJ, et al. Empagliflozin ameliorates adverse left ventricular remodeling in nondiabetic heart failure by enhancing myocardial energetics. *J Am Coll Cardiol.* 2019;73:1931–1944.
 66. Tochiya M, Makino H, Tamanaha T, Matsuo M, Hishida A, Koezuka R, Ohata Y, Tomita T, Son C, Miyamoto Y, et al. Effect of tofogliflozin on cardiac and vascular endothelial function in patients with type 2 diabetes and heart diseases: a pilot study. *J Diabetes Investig.* 2020;11:400–404.
 67. Zinman B, Wanner C, Lachin JM, Fitchett D, Bluhmki E, Hantel S, Matthews M, Devins T, Johansen OE, Woerle HJ, et al. Empagliflozin, cardiovascular outcomes, and mortality in type 2 diabetes. *N Engl J Med.* 2015;373:2117–2128. DOI: 10.1056/NEJMoa1504720.
 68. Neal B, Perkovic V, Mahaffey KW, de Zeeuw D, Fulcher G, Erondou N, Shaw W, Law G, Desai M, Matthews DR, et al. Canagliflozin and cardiovascular and renal events in type 2 diabetes. *N Engl J Med.* 2017;377:644–657. DOI: 10.1056/NEJMoa1611925.
 69. Cavaghan MK, Ehrmann DA, Polonsky KS. Interactions between insulin resistance and insulin secretion in the development of glucose intolerance. *J Clin Invest.* 2000;106:329–333. DOI: 10.1172/JCI10761.
 70. Wyse BM, Dulin WE. The influence of age and dietary conditions on diabetes in the db mouse. *Diabetologia.* 1970;6:268–273. DOI: 10.1007/BF01212237.
 71. Carroll R, Carley AN, Dyck JR, Severson DL. Metabolic effects of insulin on cardiomyocytes from control and diabetic db/db mouse hearts. *Am J Physiol Endocrinol Metab.* 2005;288:E900–E906.
 72. Myette-Cote E, Neudorf H, Rafiei H, Clarke K, Little JP. Prior ingestion of exogenous ketone monoester attenuates the glycaemic response to an oral glucose tolerance test in healthy young individuals. *J Physiol.* 2018;596:1385–1395. DOI: 10.1113/JP275709.
 73. Newman JC, Covarrubias AJ, Zhao M, Yu X, Gut P, Ng CP, Huang Y, Haldar S, Verdin E. Ketogenic diet reduces midlife mortality and improves memory in aging mice. *Cell Metab.* 2017;26:547–557.e8. DOI: 10.1016/j.cmet.2017.08.004.
 74. Borghjid S, Feinman RD. Response of C57Bl/6 mice to a carbohydrate-free diet. *Nutr Metab (Lond).* 2012;9:69. DOI: 10.1186/1743-7075-9-69.
 75. Veeranki S, Givvimani S, Kundu S, Metreveli N, Pushpakumar S, Tyagi SC. Moderate intensity exercise prevents diabetic cardiomyopathy associated contractile dysfunction through restoration of mitochondrial function and connexin 43 levels in db/db mice. *J Mol Cell Cardiol.* 2016;92:163–173. DOI: 10.1016/j.jmcc.2016.01.023.
 76. Abdurrachim D, Nabben M, Hoerr V, Kuhlmann MT, Bovenkamp P, Ciapaitė J, Geraets IME, Coumans W, Luiken JJFF, Glatz JFC, et al. Diabetic db/db mice do not develop heart failure upon pressure overload: a longitudinal in vivo PET, MRI, and MRS study on cardiac metabolic, structural, and functional adaptations. *Cardiovasc Res.* 2017;113:1148–1160. DOI: 10.1093/cvr/cvx100.
 77. Tang Y, Liu J, Long J. Phosphatase and tensin homolog-induced putative kinase 1 and Parkin in diabetic heart: role of mitophagy. *J Diabetes Investig.* 2015;6:250–255. DOI: 10.1111/jdi.12302.
 78. Tong M, Sadoshima J. Mitochondrial autophagy in cardiomyopathy. *Curr Opin Genet Dev.* 2016;38:8–15. DOI: 10.1016/j.gde.2016.02.006.
 79. Tong M, Saito T, Zhai P, Oka SI, Mizushima W, Nakamura M, Ikeda S, Shirakabe A, Sadoshima J. Mitophagy is essential for maintaining cardiac function during high fat diet-induced diabetic cardiomyopathy. *Circ Res.* 2019;124:1360–1371. DOI: 10.1161/CIRCRESAHA.118.314607.
 80. Bhansali S, Bhansali A, Walla R, Saikia UN, Dhawan V. Alterations in mitochondrial oxidative stress and mitophagy in subjects with prediabetes and type 2 diabetes mellitus. *Front Endocrinol (Lausanne).* 2017;8:347. DOI: 10.3389/fendo.2017.00347.
 81. Xiong W, Ma Z, An D, Liu Z, Cai W, Bai Y, Zhan Q, Lai W, Zeng Q, Ren H, et al. Mitofusin 2 participates in mitophagy and mitochondrial fusion against angiotensin II-induced cardiomyocyte injury. *Front Physiol.* 2019;10:411. DOI: 10.3389/fphys.2019.00411.
 82. Nie Q, Wang C, Song G, Ma H, Kong D, Zhang X, Gan K, Tang Y. Mitofusin 2 deficiency leads to oxidative stress that contributes to insulin resistance in rat skeletal muscle cells. *Mol Biol Rep.* 2014;41:6975–6983. DOI: 10.1007/s11033-014-3584-9.
 83. Uchihashi M, Hoshino A, Okawa Y, Ariyoshi M, Kaimoto S, Tateishi S, Ono K, Yamanaka R, Hato D, Fushimura Y, et al. Cardiac-specific Bdh1 overexpression ameliorates oxidative stress and cardiac remodeling in pressure overload-induced heart failure. *Circ Heart Fail.* 2017;10:e004417. DOI: 10.1161/CIRCHEARTFAILURE.117.004417.
 84. Bregere C, Rebrin I, Gallaher TK, Sohal RS. Effects of age and calorie restriction on tryptophan nitration, protein content, and activity of succinyl-CoA:3-ketoacid CoA transferase in rat kidney mitochondria. *Free Radic Biol Med.* 2010;48:609–618. DOI: 10.1016/j.freeradbiomed.2009.12.009.
 85. Nagao M, Toh R, Irino Y, Mori T, Nakajima H, Hara T, Honjo T, Satomi-Kobayashi S, Shinke T, Tanaka H, et al. Beta-hydroxybutyrate elevation as a compensatory response against oxidative stress in cardiomyocytes. *Biochem Biophys Res Commun.* 2016;475:322–328.
 86. Anderson EJ, Rodriguez E, Anderson CA, Thayne K, Chitwood WR, Kypson AP. Increased propensity for cell death in diabetic human heart is mediated by mitochondrial-dependent pathways. *Am J Physiol Heart Circ Physiol.* 2011;300:H118–H124. DOI: 10.1152/ajpheart.00932.2010.
 87. Margis R, Dunand C, Teixeira FK, Margis-Pinheiro M. Glutathione peroxidase family - an evolutionary overview. *FEBS J.* 2008;275:3959–3970. DOI: 10.1111/j.1742-4658.2008.06542.x.
 88. Le CT, Hollaar L, van der Valk EJ, van der Laarse A. Buthionine sulfoximine reduces the protective capacity of myocytes to withstand peroxide-derived free radical attack. *J Mol Cell Cardiol.* 1993;25:519–528. DOI: 10.1006/jmcc.1993.1062.
 89. Anderson EJ, Lustig ME, Boyle KE, Woodlief TL, Kane DA, Lin C-T, Price JW, Kang LI, Rabinovitch PS, Szeto HH, et al. Mitochondrial H₂O₂ emission and cellular redox state link excess fat intake to insulin resistance in both rodents and humans. *J Clin Invest.* 2009;119:573–581. DOI: 10.1172/JCI37048.
 90. Matsushima S, Kinugawa S, Ide T, Matsusaka H, Inoue N, Ohta Y, Yokota T, Sunagawa K, Tsutsui H. Overexpression of glutathione peroxidase attenuates myocardial remodeling and preserves diastolic function in diabetic heart. *Am J Physiol Heart Circ Physiol.* 2006;291:H2237–2245. DOI: 10.1152/ajpheart.00427.2006.
 91. Bhanpuri NH, Hallberg SJ, Williams PT, McKenzie AL, Ballard KD, Campbell WW, McCarter JP, Phinney SD, Volek JS. Cardiovascular disease risk factor responses to a type 2 diabetes care model including nutritional ketosis induced by sustained carbohydrate restriction at 1 year: an open label, non-randomized, controlled study. *Cardiovasc Diabetol.* 2018;17:56.
 92. Hallberg SJ, McKenzie AL, Williams PT, Bhanpuri NH, Peters AL, Campbell WW, Hazbun TL, Volk BM, McCarter JP, Phinney SD, et al. Effectiveness and safety of a novel care model for the management of type 2 diabetes at 1 year: an open-label, non-randomized, controlled study. *Diabetes Ther.* 2018;9:583–612.

SUPPLEMENTAL MATERIAL

Data S1.

Supplemental Methods

Animals and treatments

All animal handling and laboratory procedures were in accordance with the approved protocols of the Institutional Animal Care and Use Committee of the University of California, Davis conforming to the Guide for the Care and Use of Laboratory Animals published by the US National Institute of Health (8th Edition, 2011). 10-week-old male db/db mice (BKS.Cg-*Dock7*^m +/+ *Lep^r^{db}*/J, JAX#000642) and their corresponding control C57BLKS/J mice (JAX#000662) were obtained from the Jackson Laboratory (Sacramento, CA). To examine the effects of elevated KBs *in-vivo*, C57BLKS/J and db/db mice were randomly distributed in four groups. Two groups were subjected to a ketogenic diet containing 6% D- β -OHB-(R)-1,3 butanediol monoester (ketone ester, KE replacing equicaloric amounts of carbohydrate) [31] and two other groups were fed control diet.

Animals were acclimated for 4 days before the experimental diets were started. Then, all mice were trained to eat control liquid diet for 3 days, by placing feeding tubes with liquid diet in addition to chow as shown in **Figure 1A**. After the training period, the chow has been removed and all groups were switched to the corresponding liquid diets. KE diet groups were initially fed a diet containing 3% (w/v) KE for 3 days. The KE concentration in the diet was increased to 4.5% w/v after 3 days and to 6% after 6 days. The 6% KE diet was used for the remainder of the study. KE groups were fed *ad libitum*. The control diet animals were pair-fed to the KE groups, in that the control group was given the average amount of liquid diet consumed by the KE group the day before. Feeding bottles with fresh food were provided every evening, ~30 min before the start of the dark cycle.

Diets and preparations

Powdered Lieber-DeCarli diets were obtained from Bio-Serv (products F1258SP and F1259SP; Bio-Serv, Frenchtown, NJ, USA). The liquid control diet was prepared by adding warm water to the Lieber-DeCarli control diet powder. The KE diet was prepared by adding warm water to the base of the ethanol diet F1258SP but instead of ethanol, KE was added as an equicaloric replacement for maltodextrin. The composition of each diet is listed in **Table 1**. The amount of fat, proteins and total calories per gram was equal in both diets (control and KE).

Measurements of blood ketone and glucose levels

Non-fasting blood β -OHB and glucose levels were measured with commercially available colorimetric assays (Cayman Chemicals Kit #700190 for β -OHB and Sigma High Sensitivity Assay kit MAK181 for glucose) according to the manufacturer's instructions. During feeding experiments non-fasting blood glucose and β -OHB levels were periodically checked with glucose and ketone sticks using a Precision Xtra meter (Abbott Laboratories, Abbott Park, IL, USA).

Echocardiography

Cardiac function was examined using 2D echocardiography using a VisualSonics Vevo 2100 echocardiography machine (VisualSonics, Toronto, ON, Canada) and a MS 550D probe (22-55 MHz) under anesthesia with 1%-1.5% isoflurane in a 100% O₂ atmosphere gas chamber. Some recordings were performed in conscious animals to verify the effect of anesthesia on cardiac function (see **Figures S1 and S2**). Fractional shortening (FS), ejection fraction (EF), stroke volume, and cardiac output were calculated from the M-mode images. LV mass was calculated using M-mode data as reported by Troy [37] using the following equation $LV\ mass\ (AW) = 1.05 ([LVIDD + LVPWT + IVSD]^3 - [LVIDD]^3)$, where LVIDD is LV internal diameter at diastole, LVPWT is LV posterior wall thickness at diastole and IVSD is intraventricular septum thickness at diastole.

Doppler imaging was performed to determine peak velocity during rapid filling phase in early diastole (E wave), and peak filling velocity in late diastole as a result of atrial contraction (A wave), and E/A ratios. Tissue doppler imaging was performed to calculate E/e' ratio.

Morphometric measurements

Four weeks after diet intervention, mice were anesthetized in a gas chamber with 3-5% isoflurane in a 100% O₂ atmosphere and sacrificed. Each animal was euthanized by exsanguination under deep anesthesia. Hearts and lungs were excised, blotted dry, and weighed. Tibial length (TL) was measured with vernier calliper and used to normalize heart/lungs weights. Increased cardiac mass was evaluated by examining the ratios between heart weight-to-tibial length. Pulmonary congestion was examined by calculating lungs weight-to-tibial length ratios.

Western blotting

Hearts were homogenized in ice-cold RIPA lysis buffer and protein content was measured using the BCA method. Blocked membranes were incubated with primary antibodies towards total BDH1 (Abcam ab193156), OXCT1 (SCOT, Abcam ab105320), and ACAT1 (Abcam ab168342). Membranes were scanned using the Licor Odyssey infrared imaging system and analyzed with ImageJ software. Band intensities of all samples were normalized to the internal housekeeping proteins (GAPDH, Abcam ab8245 or α -tubulin, Abcam ab7291) that were included on each gel.

Some experiments were performed using Jess capillary western blot system according to the manufacturer specifications (Protein Simple, San Jose, CA). Briefly, tissue lysates were loaded in 24 well Protein Simple plates together with primary antibodies (Total OXPHOS Rodent WB Antibody Cocktail, Abcam ab110413 and VDAC1 (Abcam ab15895), secondary antibodies (anti-mouse NIR and anti-rabbit HRP from Protein Simple), protein normalizing reagent, and chemiluminescent substrates. Proteins were separated within individual capillaries using Protein Simple cartridges. The signal intensity was analyzed as area under the curve for each protein peak using Protein Simple Software and normalized to total protein or loading control of interest. Digital images were generated for visual representation of the signal. For the antioxidant enzymes, primary antibodies against catalase (ab16731), thioredoxin/TRX (ab273877), superoxide dismutase 1/SOD1 (ab51254) and glutathione peroxidase 4/GPX4 (ab125066) were used. Data were normalized to GAPDH loading control (ab8245). For mitophagy studies, primary antibodies against PINK1 (Abcam ab23707), Parkin (Abcam ab15954), mitofusin 2 (ab124773), SQSTM1/p62 (Abcam ab56416), and LC3 (Abcam ab192890) were used. GAPDH (Abcam ab9483) was used as loading controls.

Mitochondrial respiratory chain coupling and electron flux

Mitochondria were isolated using a standard differential centrifugation method [5]. Briefly, minced hearts were placed in mitochondrial isolation buffer (IB₁) in 67 mM sucrose, 50 mM Tris/HCl, 50 mM KCl, 10 mM EDTA, and 0.2% BSA with a pH=7.2, homogenized with a glass Teflon pestle, and subsequently centrifuged at 700g for 10 min at 4°C. The supernatant was collected and centrifuged at 8,000g for 10 min at 4°C. The pellet was then resuspended in ice-cold buffer (IB₂) containing 250 mM sucrose, 3 mM EGTA/Tris, and 10 mM Tris/HCl with a pH=7.2, followed by centrifugation at 8,000g for 10 min at 4°C. Mitochondria were then re-suspended and stored in IB₂. Protein concentration was determined using the Bradford Assay. Coupling and electron flux assays were performed as described [38].

Cell Isolation

Hearts were excised from adult db/db and age- and strain-matched WT mice. Hearts were placed on a Langendorff-perfusion apparatus and perfused for 6 minutes at 37°C with nominally Ca²⁺-free Dulbecco's modified Eagle's medium (DMEM; GIBCO type 22300) gassed with a 95% O₂/5% CO₂ mixture. Perfusion was then switched to the same solution containing Liberase TM (Research Grade, Roche) and 20 μmol/L Ca²⁺ with perfusion continuing until the heart became flaccid (~7-12 minutes). Atria were removed, enzyme activity was blocked by switching the solution to DMEM containing 0.5% to 1% BSA, and the ventricles were cut into smaller pieces and gently pushed up and down with a plastic transfer pipette to separate individual cells. Isolated cells were kept in MEM solution with 50 μmol/L Ca²⁺ at room temperature (22–24°C) until used for experimentation or placed in a short-term culture (see below). For confocal measurements, isolated cardiomyocytes were plated on glass coverslips with laminin coating. All experiments were performed at room temperature (22-24°C).

Mitochondrial membrane potential ($\Delta\Psi_m$) measurements

Mitochondrial membrane potential ($\Delta\Psi_m$) was measured in intact freshly isolated cardiomyocytes using the potentiometric probe tetramethylrhodamine methylester (TMRM) ($\lambda_{ex} = 543$ nm and $\lambda_{em} = 565$ – 605 nm) [39-42].

Mitochondrial permeability transition pore (mPTP) activity

mPTP activity was measured in permeabilized cells incubated with 5 μM calcein/AM (λ_{ex} =488 nm, λ_{em} =510 nm) for 40 min at 37°C [39, 43-45]. Opening of mPTP induces the loss of mitochondria-trapped calcein (620 Da) and a decrease of fluorescence. At the end of each recording 10 μg/ml of the pore-forming antibiotic alamethicin was added to obtain a maximum calcein release from mitochondria for data normalization

Oxidative stress and redox measurements in cultured murine cardiomyocytes

To examine oxidative stress in db/db and corresponding control cardiomyocytes, we employed adenoviral construct to express redox-sensitive green fluorescent protein 2 (roGFP2) fused to specific sensor domains to measure changes in hydrogen peroxide (H₂O₂) either in mitochondria or cytosol of intact cells [27, 46]. For this sensor to be specific for H₂O₂, the redox-sensitive roGFP2 was fused with the yeast peroxidase ORP1 [47]. When ORP1 reacts with H₂O₂, it forms

a cysteine sulfenic acid (Cys-SOH) in the active site, leading to the formation of protein disulfide bonds in roGFP2, thus shifting the 405/488-nm excitation ratio [47].

To monitor redox changes inside cytosol and mitochondria, a fusion construct roGFP2-GRX1 was employed. roGFP2-GRX1 uses human glutaredoxin to sense the changes in oxidized glutathione (GSSG) relative to the level of reduced glutathione (GSH), GSSG/GSH [48-50]. To calibrate the signal, diamide was added at the end of each experiment to oxidize the GSH pool and obtain R_{\max} for the roGFP2 probe and DTT to obtain R_{\min} . Mitochondrial targeting of both constructs was obtained by fusion of roGFP2-ORP1/roGFP2-GRX1 to the mitochondrial targeting sequence of the first 69 amino acids of subunit 9 of the F_0 -ATPase of *Neurospora crassa* [51]. Both constructs were excited with the 405- and 488-nm laser lines, and emission was detected at 510 nm. These two excitation peaks have different redox dependence where cysteine oxidation induces increase in 405 nm excitation peak and a corresponding decrease in 488 nm excitation peak while cysteine reduction has an inverse effect. Therefore, the ratio in emission recorded at 405 nm to 488 nm excitation wavelengths is used as a measure of the relative amount of oxidized to reduced roGFP2 [49, 50].

To express these adenoviral constructs, freshly isolated cardiomyocytes were placed in a short term (24-48h) culture in MEM (Invitrogen) supplemented with 2 mM Glutamine, 1X Insulin (1 mg/ml)-transferrin (0.55 mg/ml)-selenium (0.67 ng/ml), 0.2% Bovine serum albumin, 4 mM NaHCO_3 , 10 mM HEPES, 100 U/ml Penicillin-streptomycin, and 25 μM Blebbistatin. 2 mM β -OHB was added to the medium of KE treated groups to maintain the elevated β -OHB concentration during cell culture.

Mitochondrial Redox State

Flavin adenine dinucleotide (FAD)-linked protein autofluorescence ($\lambda_{\text{ex}} = 488 \text{ nm}$, $\lambda_{\text{em}} = 510 \text{ nm}$) was used as another measure of the mitochondrial redox state in freshly isolated cardiomyocytes [44]. Data are presented as the ratio of oxidized FAD to reduced FADH_2 (FAD/FADH_2) calculated as $(F - F_{\min}) / (F_{\max} - F_{\min})$ where F is the fluorescence intensity recorded from the mitochondrial regions of interest. F_{\min} is the fluorescence obtained after addition of 4 mM NaCN (inhibits respiration and promotes maximal FAD reduction, i.e. FADH_2 formation), taken as 0%. F_{\max} is the fluorescence obtained after addition of 4 μM FCCP (stimulates maximal respiration, completely oxidizing the mitochondrial FADH_2 pool), taken as 100%.

Mitophagy Markers Measurements

To measure Parkin accumulation in mitochondria and LC3-mediated autophagosome formation, mCherry-Parkin and GFP-LC3 were expressed in cardiomyocytes via adenoviral gene transfer as previously described [27, 52]. Culturing conditions were the same as described above for redox sensitive constructs. mCherry-Parkin fluorescence was excited at 540 nm and monitored at 590 nm while GFP-LC3 fluorescence was measured with $\lambda_{\text{ex}}=488 \text{ nm}$ and $\lambda_{\text{em}}=510 \text{ nm}$.

Statistical Analysis

All data were analyzed using unpaired t-tests or two-way analysis of variance (ANOVA) with Bonferroni's post-hoc, using GraphPad Prism version 7.0 (Graph-Pad Software Inc., San Diego, USA) and $p < 0.05$ was considered statistically significant. All data are shown as mean \pm standard error of the mean (SEM).

Table S1. Statistics table reflecting P-values for genotype, diet comparison, and the interaction factor.

Figure Number	Genotype P-value	Diet P-value	Interaction P-value
Figure 1D	0.0168	<0.0001	0.0678
Figure 1E	<0.0001	<0.0001	0.0002
Figure 1F	<0.0001	0.0322	0.4186
Figure 1G	<0.0001	0.1741	0.1232
Figure 1I	<0.0001	0.2076	0.6701
Figure 2D	0.0036	0.0205	0.1706
Figure 2F	<0.0001	0.2709	0.2203
Figure 2I	0.0329	0.0010	0.0278
Figure 2L	0.2255	0.0049	0.1286
Figure 2M	0.0083	0.1012	0.0153
Figure 2N	0.0014	0.0107	0.1919
Figure 2P	<0.0001	0.0257	0.0660
Figure 2Q	0.0869	0.0256	0.0232
Figure 3C	0.0798	0.2041	0.0124
Figure 3D	0.2270	<0.0001	0.6657
Figure 3E	0.0008	0.0062	0.2999
Figure 4B (Pyruvate/Malate)	0.0003	<0.0001	0.6596
Figure 4B (Succinate)	<0.0001	<0.0001	0.5113
Figure 4B (TMPD/Asc)	0.0041	<0.0001	0.3057
Figure 4D (Basal)	0.0005	0.0413	0.4630
Figure 4D (State 3)	<0.0001	0.0205	0.4743
Figure 4D (State 4 _o)	<0.0001	0.0203	0.730
Figure 4D (3 _u)	0.0004	0.4522	0.1008
Figure 4E	<0.0001	<0.0001	0.8457
Figure 4F	<0.0001	0.0007	0.3620
Figure 4G	0.4174	0.0239	0.9793
Figure 5B	0.0656	0.0016	0.0070
Figure 5C	0.9695	0.0014	0.6443
Figure 5D	0.5413	0.1332	0.0164
Figure 5E	0.0286	0.0088	0.1718
Figure 5F	0.0017	<0.0001	0.6
Figure 5G	0.0139	0.0574	0.0567
Figure 6C	<0.0001	<0.0001	<0.0001
Figure 6D	<0.0001	<0.0001	<0.0001
Figure 6E	<0.0001	<0.0001	<0.0001
Figure 6F	<0.0001	<0.0001	0.0101
Figure 6G	<0.0001	0.0163	0.0492

Figure 6H	<0.0001	0.0003	0.0686
Figure 6J	0.0001	0.1717	<0.0001
Figure 6K	0.0046	<0.0001	0.1934
Figure 6N	0.0011	0.0630	0.0015
Figure 7C	0.0682	<0.0001	0.3950
Figure 7E (2 mM)	0.0335	0.0047	0.0117
Figure 7E (50 mM)	<0.0001	0.0017	0.0964
Figure 7G (FS)	<0.0001	<0.0001	<0.0001
Figure 7G (FS+ISO)	<0.0001	<0.0001	<0.0001
Figure 8D	<0.0001	<0.0001	<0.0001
Figure 8E	<0.0001	<0.0001	0.0087
Figure 8F	0.0046	0.1195	0.0253
Figure 8G	0.3930	<0.0001	<0.0001
Figure 8H	0.3938	<0.0001	<0.0001
Figure 8I	0.1843	<0.0001	0.0003

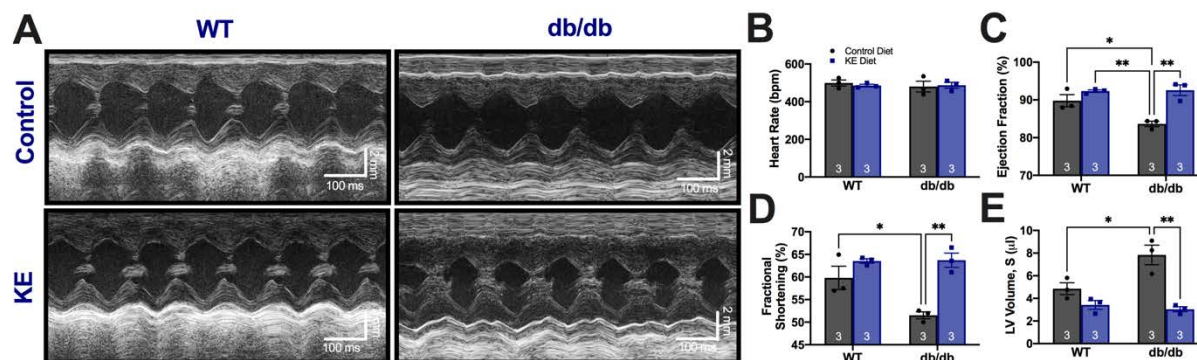


Figure S1. Echocardiography measurement in conscious animals. (A) Shown are the representative M-mode echocardiography recordings performed in conscious animals to evaluate the systolic function of the heart. (B) Heart rate measurements in control (WT) and diabetic heart (db/db) fed control (grey) and KE (blue) diet, (C) Changes in ejection fraction in control (WT) and diabetic heart (db/db) fed control (grey) and KE (blue) diet, (D) Changes in fractional shortening in control (WT) and diabetic heart (db/db) fed control (grey) and KE (blue) diet, and (E) LV volume measurements during systole in control (WT) and diabetic heart (db/db) fed control (grey) and KE (blue) diet. Data expressed as mean±SEM with n as the number of mice in the bar graphs. *p<0.05 and **p<0.01 were calculated using two-way analysis of variance (ANOVA) with Tukey's post hoc multiple comparison.

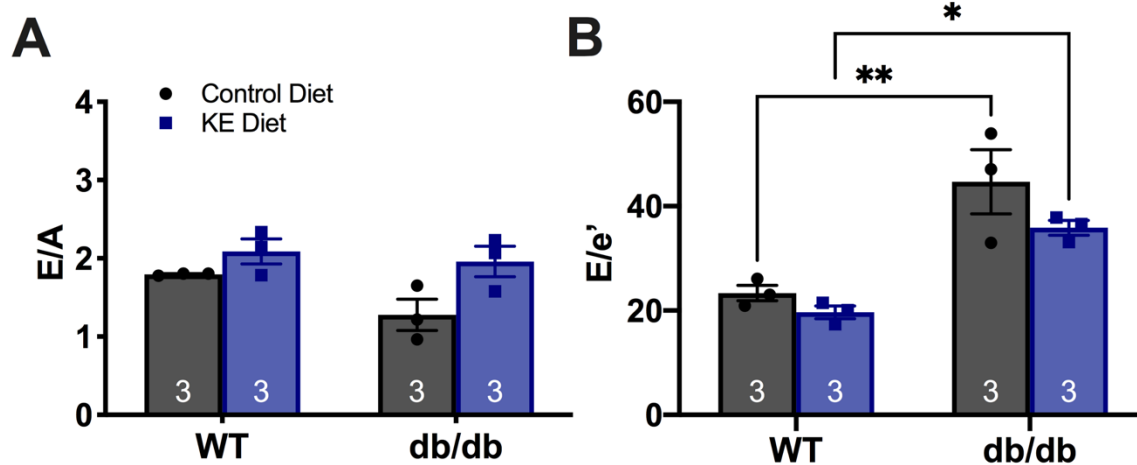


Figure S2. Cardiac diastolic parameters recorded in conscious animals using in-vivo echocardiography. Shown are (A) mitral valve E/A ratio, and (B) E/e' ratio measured in control (WT) and diabetic heart (db/db) fed control (grey) and KE (blue) diet. Data are expressed as mean±SEM with n as the number of mice in the bar graphs. *p<0.05 and **p<0.01 were calculated using two-way analysis of variance (ANOVA) with Tukey's post hoc multiple comparison.

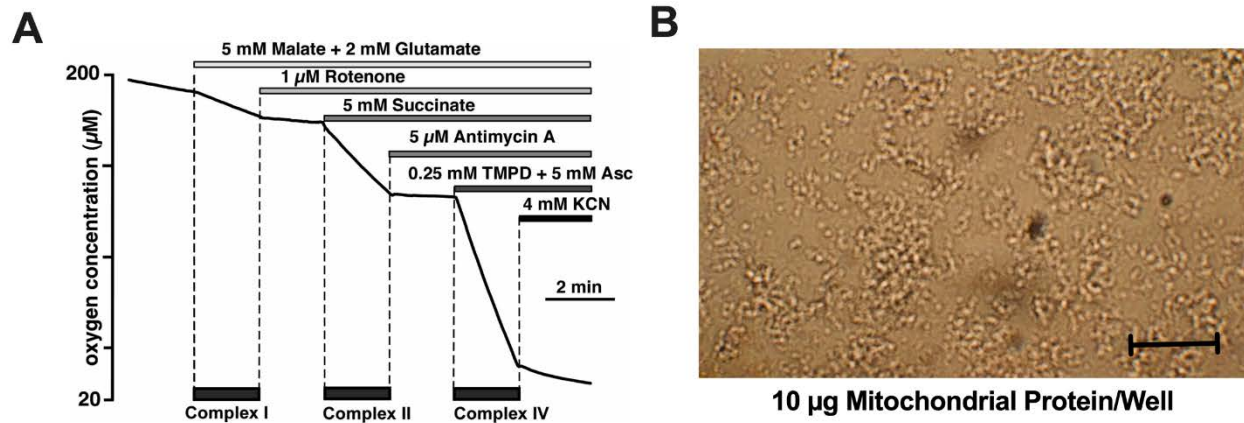


Figure S3. (A) Changes in oxygen concentration recorded with oxygen-sensitive Clark type electrode during subsequent addition of mitochondrial substrates and inhibitors for mitochondrial complex I, II, and IV, respectively. (B) 10 micrograms of mitochondria were loaded into each well of the Seahorse plate. A representative image of mitochondria located inside of a well of 24-well Seahorse plate is shown. The bar graph corresponds to 10 μm .

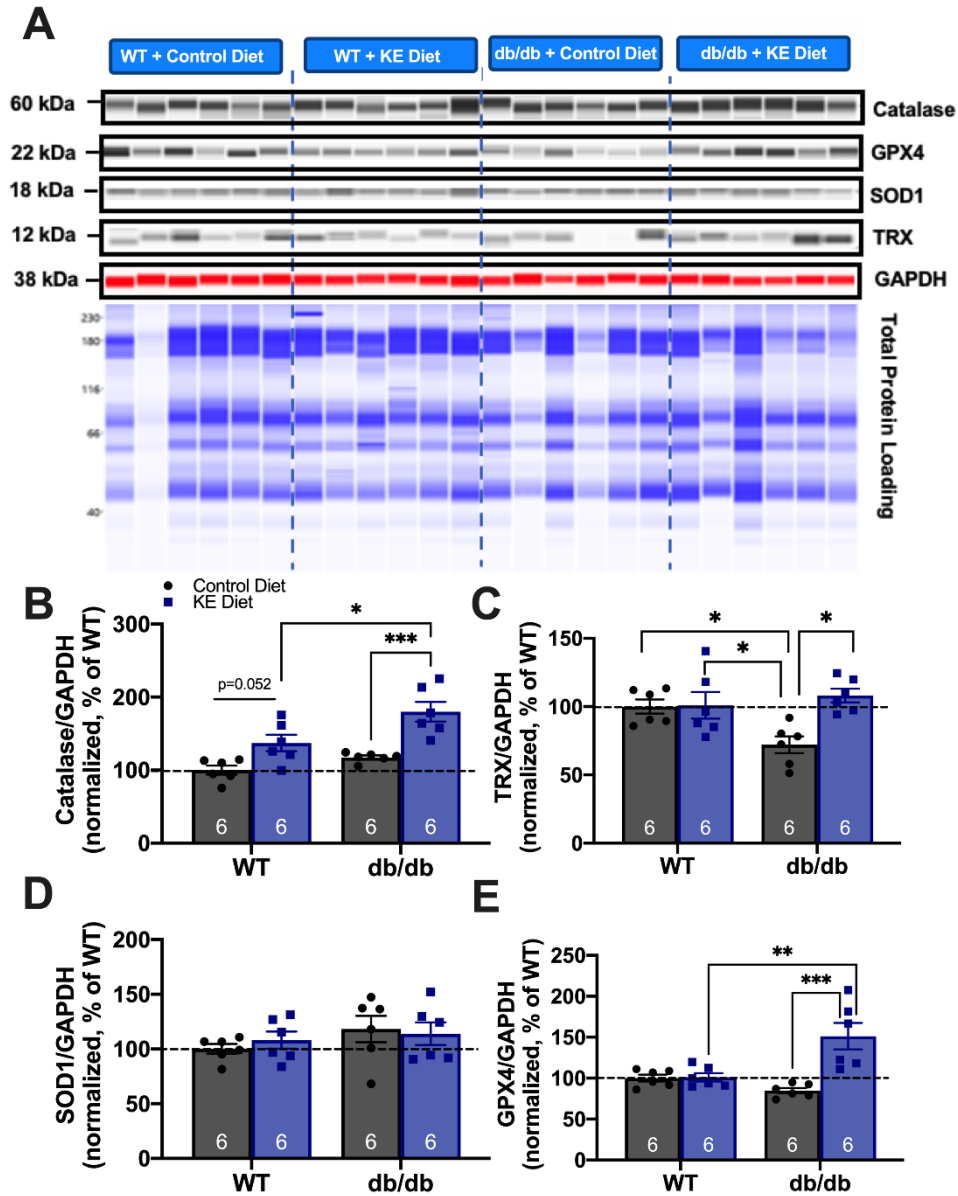


Figure S4. (A) Expression of the proteins involved in oxidative stress defense in cardiac tissues from WT and diabetic (db/db) hearts on control and ketone ester (KE) diet: catalase, thioredoxin (TRX), superoxide dismutase 1 (SOD1), and glutathione peroxidase 4 (GPX4), respectively. GAPDH staining was used to confirm equal protein loading for each experimental group. Total protein loading was verified with Protein Normalization reagent (blue). Data were obtained with the capillary Jess Western blot technology. (B-E) Area under the curve for each protein was analyzed and data are expressed as a percent change of WT+Control Diet group for catalase, thioredoxin (TRX), superoxide dismutase 1(SOD1), and glutathione peroxidase 4 (GPX4). Data expressed as mean±SEM with n as the number of samples in the bar graphs. *p<0.05, **p<0.01, and ***p<0.001 were calculated using two-way analysis of variance (ANOVA) with Tukey's post hoc multiple comparison.

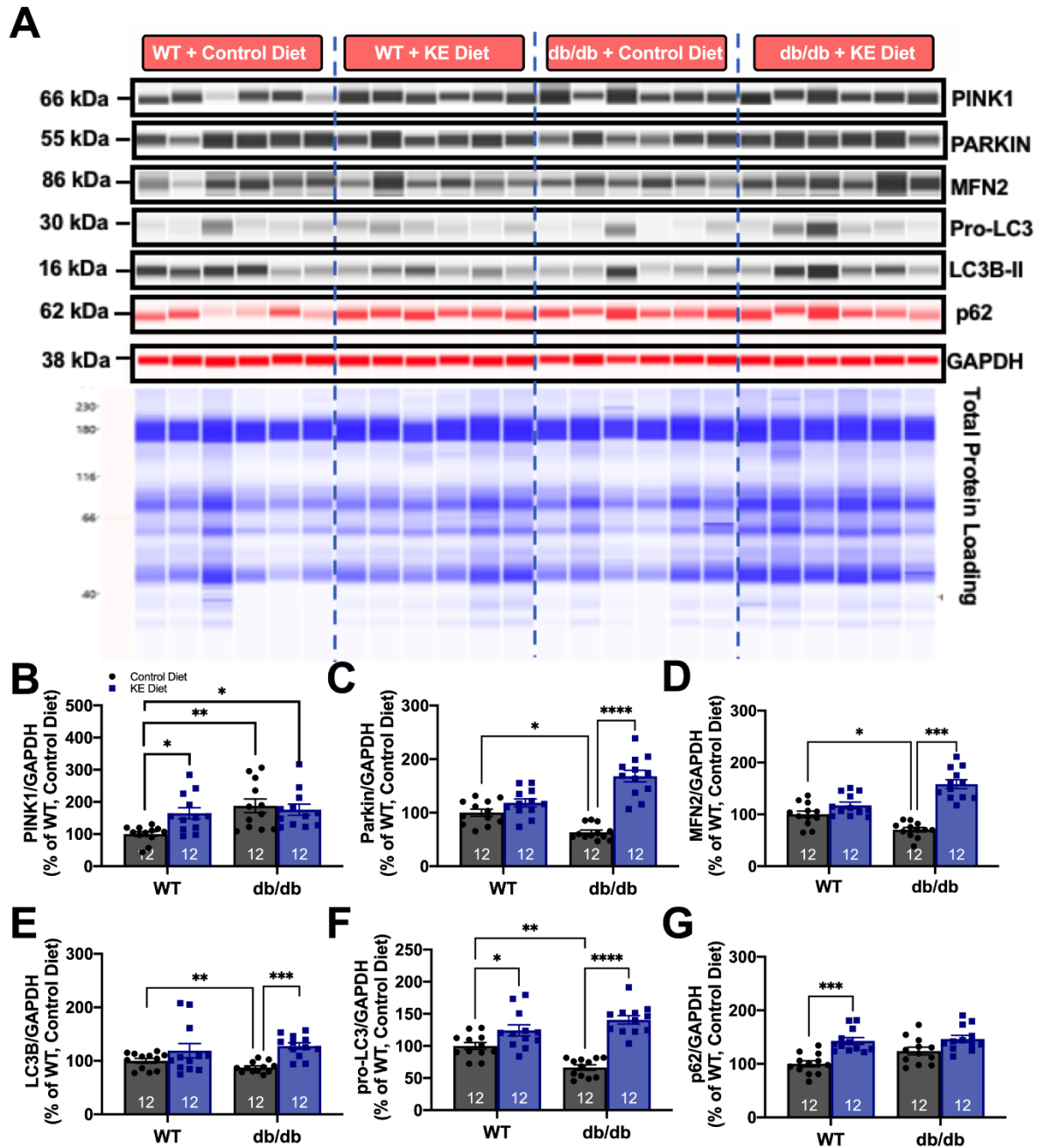


Figure S5. (A) Expression of the proteins in PINK-Parkin mitophagy pathway in cardiac myocytes from WT and diabetic (db/db) hearts on control and ketone ester (KE) diet: PINK-1, Parkin, mitofusin 2 (Mfn2), pro-LC3, LC3B-II, and p62. GAPDH staining was used to confirm equal protein loading for each experimental group. Total protein loading was verified with Protein Normalization reagent (blue). Data were obtained with the capillary Jess Western blot technology. (B-G) Area under the curve for each protein was analyzed and data are expressed as a percent change of WT+Control Diet group for PINK-1, Parkin, Mfn2, LC3B-II, pro-LC3 and p62. Data expressed as mean \pm SEM with n as the number of samples in the bar graphs. * $p < 0.05$, ** $p < 0.01$, *** $p < 0.001$, and **** $p < 0.0001$ were calculated using two-way analysis of variance (ANOVA) with Tukey's post hoc multiple comparison.